

# Nonlinear analysis of viscoelastic micro-composite beam with geometrical imperfection using FEM: MSGT electro-magneto-elastic bending, buckling and vibration solutions

S. Alimirzaei<sup>1</sup>, M. Mohammadimehr<sup>\*1</sup> and Abdelouahed Tounsi<sup>2,3</sup>

<sup>1</sup>Department of Solid Mechanics, Faculty of Mechanical Engineering, University of Kashan, P.O. Box: 87317-51167, Kashan, Iran

<sup>2</sup>Department of Civil and Environmental Engineering, King Fahd University of Petroleum & Minerals, 31261 Dhahran, Eastern Province, Saudi Arabia

<sup>3</sup>Material and Hydrology Laboratory, Faculty of Technology, Civil Engineering Department, University of Sidi Bel Abbes, Algeria

(Received January 22, 2019, Revised March 14, 2019, Accepted March 16, 2019)

**Abstract.** In this research, the nonlinear static, buckling and vibration analysis of viscoelastic micro-composite beam reinforced by various distributions of boron nitrid nanotube (BNNT) with initial geometrical imperfection by modified strain gradient theory (MSGT) using finite element method (FEM) are presented. The various distributions of BNNT are considered as UD, FG-V and FG-X and also, the extended rule of mixture is used to estimate the properties of micro-composite beam. The components of stress are dependent to mechanical, electrical and thermal terms and calculated using piezoelectricity theory. Then, the kinematic equations of micro-composite beam using the displacement fields are obtained. The governing equations of motion are derived using energy method and Hamilton's principle based on MSGT. Then, using FEM, these equations are solved. Finally the effects of different parameters such as initial geometrical imperfection, various distributions of nanotube, damping coefficient, piezoelectric constant, slenderness ratio, Winkler spring constant, Pasternak shear constant, various boundary conditions and three material length scale parameters on the behavior of nonlinear static, buckling and vibration of micro-composite beam are investigated. The results indicate that with an increase in the geometrical imperfection parameter, the stiffness of micro-composite beam increases and thus the non-dimensional nonlinear frequency of the micro structure reduces gradually.

**Keywords:** nonlinear bending; buckling; vibration analysis; viscoelastic beam; various distributions of BNNTs; initial geometrical imperfection; MSGT; FEM

## 1. Introduction

Functionally graded materials (FGMs) are a novel generation of composites that exhibit continuous and smooth distribution in material characteristics from one surface to another, helping to reduce stress concentrations in laminated composites. The concept of FGM can be used effectively for a better management of the microstructure of the material in a beam/plate structure reinforced by CNT to improve the mechanical behavior. The addition of BNNT or CNT with FGM provides enhanced mechanical, electrical and thermal properties, as well as an additional advantage in achieving the desired properties by varying the distribution and composition of the BNNTs or CNTs (Liew *et al.* 2015, Mohammadimeh *et al.* 2016a, Mehar and Panda 2017, Bakhadda *et al.* 2018, Ghorbanpour Arani and Amir 2013).

The design of micro and nano-electro-mechanical systems (MEMS / NEMS) at the micro or nano dimension requires the widely use of micro-structures with many complex behaviors. Thus, it is important to consider the scale influences in their mechanical responses. Wang *et al.* (2015) presented a wave propagation study in nonlinear

curved single-walled CNTs by considering a nonlocal elasticity theory. By employing DQM, Murmu and Pradhan (2009) discussed the buckling behavior of a SWCNT embedded in an elastic medium based on nonlocal elasticity and Timoshenko beam model. Bellifa *et al.* (2017) proposed a nonlocal zeroth-order shear deformation theory for nonlinear post-buckling of nano-beams. Using a nonlocal Euler-Bernoulli beam model, Narendar *et al.* (2012) investigated the wave propagation in SWCNT under longitudinal magnetic field. Mohammadimehr *et al.* (2016b) presented both vibration and wave propagation study of twisted micro-beam via strain gradient theory. Zhang *et al.* (2014) proposed a new Timoshenko beam element based on the strain gradient elasticity theory for the investigation of the bending, dynamic and stability responses of Timoshenko micro-beams. Wang *et al.* (2013) analyzed the nonlinear vibration of embedded SWCNT with geometrical imperfection subjected to harmonic force by considering a nonlocal Timoshenko beam theory. Using differential quadrature method (DQM), Mohammadimehr *et al.* (2016c) studied the size-dependent influence on biaxial and shear nonlinear stability behavior of nonlocal isotropic and orthotropic micro-plate based on surface stress and modified couple stress models. Karami *et al.* (2018a) presented a nonlocal strain gradient 3D elasticity theory for anisotropic spherical nano-particles. Based on a novel

\*Corresponding author, Ph.D.

E-mail: mmohammadimehr@kashanu.ac.ir

nonlocal strain gradient higher order shell theory, Karami *et al.* (2018b) proposed a variational formulation for wave dispersion in anisotropic doubly-curved nano-shells.

Investigations on the bending, vibration and buckling response of composite structures reinforced by BNNTs or CNTs are one of the considerable topics in structural mechanics. Vaccarini *et al.* (2000) provided mechanical and electronic properties of CNTs and BNNTs. Mosallaie Barzoki *et al.* (2012) considered the electro-mechanical torsional buckling of a piezoelectric polymeric shell reinforced by double walled boron nitride nanotubes (DWBNTs). The results of their research showed that the buckling strength increases substantially as harder foam cores are employed. Nirmala and Kolandaivel (2007) investigated structure and electronic properties of armchair BNNTs as a function of tube diameter using density functional theory. The Young's moduli and the Poisson's ratio of the boron-nitride crystals determined by the continuum approach were comparable to both experimental and theoretical ones by Oh (2011s). Salehi-Khojin and Jalili (2008) studied the stability of BNNT reinforced piezoelectric polymeric composites under electrothermo-mechanical loadings. Mohammadimehr *et al.* (2015) investigated the dynamic behavior of visco-elastic double-bonded polymeric nano-composite plates reinforced by FG-SWCNTs employing MSGT, sinusoidal shear deformation model and meshless technique. Using finite element method, Mohammadimehr and Alimirzaei (2017) discussed the buckling and free vibration response of tapered FG-CNTRC micro Reddy beam subjected to longitudinal magnetic field. Mohammadimehr and Alimirzaei (2016) presented nonlinear static and vibration investigation of Euler-Bernoulli composite beam model reinforced by FG-SWCNT by considering initial geometrical imperfection via FEM. Yas and Samadi (2012) analyzed the dynamic and buckling behavior of CNT-reinforced composite Timoshenko beams resting on elastic foundation. Heshmati and Yas (2016) studied the dynamic response of FG multi-walled carbon nanotube-polystyrene nano-composite beams under multi-moving loads. Mohammadimehr *et al.* (2016) employed a modified strain gradient Reddy rectangular plate model for biaxial stability and bending investigation of double-coupled piezoelectric polymeric nano-composite reinforced by FG-SWNT. Mohammadimehr *et al.* (2013) studied flexural static, buckling, and dynamic behaviors of MSGT micro-composite Reddy plate reinforced by FG-SWCNTs with temperature-dependent material properties subjected to hydro-thermo-mechanical loadings by employing DQM. Ghorbanpour Arani *et al.* (2015) discussed the surface stress and agglomeration influences on nonlocal biaxial stability polymeric nano-composite plate reinforced by CNT by utilizing various formulations. Liew *et al.* (2014) analyzed post-buckling of carbon nanotube-reinforced FG cylindrical panels under axial compression via a meshless approach. Yas and Heshmati (2012) presented a dynamic investigation of FG nano composite beams reinforced by randomly oriented CNT subjected to a moving load. Moradi *et al.* (2013) analyzed the dynamic behavior of FG nano-composite cylinders reinforced by CNT by a mesh-free method. Zhang and Selim (2015 and 2017) used element-free improved moving least square (IMLS)-Ritz method developed for studying vibration analysis of CNT-reinforced thick composite plates

based on Reddy's higher-order shear deformation theory. Also, numerical methods have been used to calculate the normal stress in laminated carbon nanotube-reinforced functionally graded composite plates (2016a), piezoelectric and anisotropic multilayer composites in Reddy's plate (2016). Zhang *et al.* (2013, 2016b, 2016c and 2016d) and Zhu *et al.* (2014) studied thermal and mechanical analysis of functionally graded plates using a numerical method. Also, some researchers worked about composite, nano and micro composite and various size dependent effect in the literature (Ghorbanpour Arani *et al.*, 2011a, b, 2012; Mohammadimehr and Rahmati, 2013, Mohammadimehr *et al.* 2010, 2013, 2016f, 2017a, b,c).

Although nonlinear analysis is studied widely in micro-composite beam, to date no report has been found in the literature on nonlinear analysis of the embedded viscoelastic micro composite beam with initial geometrical imperfection using FEM. This research has the aim to investigate, the nonlinear static, buckling and vibration, analysis of micro composite beam reinforced by various distributions of BNNT using MSGT. In order to present a realistic model, the material properties of the system are assumed to be viscoelastic which are characterized by using Kelvin Voigt model. Timoshenko beam theory is applied for obtaining the motion equations. Finally, using FEM, the bending, buckling and natural frequencies of micro composite beam are calculated. Also the influences of the various parameters such as initial geometrical imperfection, different distributions of nanotube, damping coefficient, piezoelectric constant, slenderness ratio, Winkler spring constant, Pasternak shear constant, various boundary conditions and three material length scale parameters on the behavior of bending, buckling and vibration of non-linear micro composite beam are investigated.

## 2. Geometry

According to Fig. 1a, the Timoshenko micro composite beam under electro-thermo-mechanical loadings is considered with length  $L$ , width  $b$  and thickness  $h$ . This micro composite beam rested on elastic foundation with Winkler coefficient  $K_w$  and Pasternak shear coefficient  $K_g$ . Fig. 1b shows the various distributions of FG-SWBNTs in micro composite Timoshenko beam. UD is uniform distribution of nanotube. USFG and SFG denote unsymmetrical and symmetrical functionally graded distributions of nanotube, respectively, that are famous to FG-V (functionally graded V distribution of nanotube) and FG-X (functionally graded V distribution of nanotube) and are assumed to reinforce the micro composite beam. Volume fraction for these distributions is defined as follows (Yas and Samad 2012, Yas and Heshmati 2012)

$$V_{BNNT}(z) = \begin{cases} V_{BNNT}^* & UD \\ \left(1 - \frac{2z}{h}\right) V_{BNNT}^* & FG-V (USFG) \\ 2\left(\frac{2|z|}{h}\right) V_{BNNT}^* & FG-X (SFG) \end{cases} \quad (1-a)$$

where

$$V_{BNNT}^* = \frac{W_{BNNT}}{W_{BNNT} + \left(\frac{\rho_{BNNT}}{\rho_m}\right) - \left(\frac{\rho_{BNNT}}{\rho_m}\right)W_{BNNT}} \quad (1-b)$$

$W_{BNNT}$ ,  $\rho_{BNNT}$  and  $\rho_m$  are mass fraction of BNNT, density of BNNT and matrix, respectively.

### 3. The extended rule of mixture

According to the extended rule of mixture model, the effective Young’s modulus, shear modulus, Poisson’s ratio and mass density of FG-SWBNT Timoshenko beams can be expressed as follows (Mohammadimehr *et al.* 2016, Yas and Heshmati 2012)

$$\begin{aligned} E_{11} &= \eta_1 V_{BNNT} E_{11}^{BNNT} + V_m E_m \\ \frac{\eta_2}{E_{22}} &= \frac{V_{BNNT}}{E_{22}^{BNNT}} + \frac{V_m}{E_m} \\ \frac{\eta_3}{G_{12}} &= \frac{V_{BNNT}}{G_{12}^{BNNT}} + \frac{V_m}{G_m} \\ \rho &= V_{BNNT} \rho_{BNNT} + V_m \rho_m \\ \nu_{12} &= V_{BNNT} \nu_{BNNT} + V_m \nu_m \end{aligned} \quad (2)$$

where  $E_{11}^{BNNT}$ ,  $E_{22}^{BNNT}$ ,  $G_{12}^{BNNT}$ ,  $\nu_{BNNT}$ ,  $\rho_{BNNT}$  and  $E_m$ ,  $G_m$ ,  $\nu_m$ ,  $\rho_m$  indicate the Young’s modulus, shear modulus, Poisson’s ratios and density of BNNT and matrix, respectively.  $\eta_i$  ( $i=1,2,3$ ) denotes force transformation between FG-SWBNTs and polymeric matrix.

### 4. Governing equations of micro composite viscoelastic Timoshenko beam

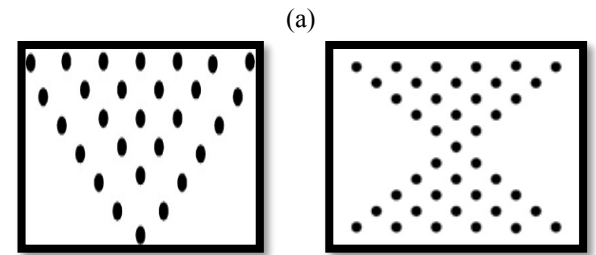
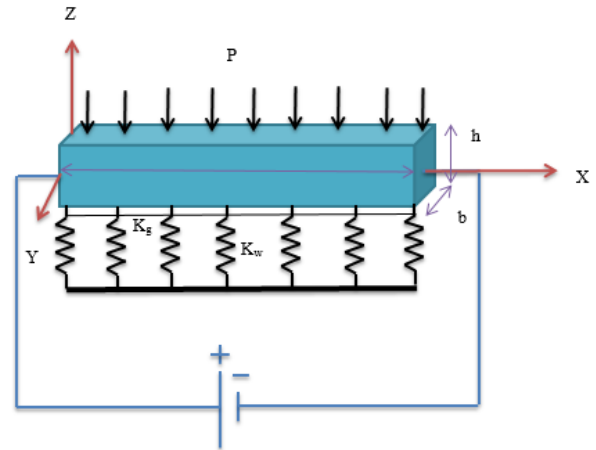
Displacements field of the FG-SWBNT micro composite beam can be written as follows (Yas and Heshmati 2012, Adnan Elshafei 2013)

$$\begin{aligned} u_1(x, y, z, t) &= u(x, t) - z \left[ c_0 \frac{dw}{dx} + c_1 \psi(x, t) \right] \\ &+ c_2 z^2 \phi(x, t) + c_3 \left( \frac{z}{h} \right)^3 \left[ \frac{dw}{dx} + \psi(x, t) \right] \\ u_3(x, y, z, t) &= w(x, t) \quad ; \quad u_2(x, y, z, t) = 0 \end{aligned} \quad (3)$$

where  $u_1$ ,  $u_2$  and  $u_3$  represent components of displacement vector in  $x$ ,  $y$  and  $z$  directions, respectively, and  $u$  and  $w$  denote the displacements on the mid-plane along  $x$  and  $z$  directions, respectively. Also  $\psi(x, t)$  and  $\phi(x, t)$  are the rotation angles of the cross-section. The coefficient of  $c_0$ ,  $c_1$ ,  $c_2$  and  $c_3$  for Timoshenko beam theory is defined as follows:

$$c_0 = 0, c_1 = 1, c_2 = 0, c_3 = 0 \quad (4a)$$

Substituting Eq. (4a) into Eq. (3), the displacement field for Timoshenko beam is obtained



Unsymmetrical functionally graded distribution of nanotube (USFG or FG-V)

Symmetrical functionally graded of nanotube (SFG or FG-X)

$$V_{BNNT}(z) = \left(1 - \frac{2z}{h}\right) V_{BNNT}^* \quad V_{BNNT}(z) = 2 \left(\frac{2|z|}{h}\right) V_{BNNT}^*$$

(b)

Fig. 1 a) A schematic view of micro composite beam under electro-thermo-mechanical loadings embedded in an elastic foundation b) A schematic view of unsymmetrical and symmetrical functionally graded distributions of nanotube

$$\begin{cases} u_1(x, y, z, t) = u(x, t) + z\psi(x, t) \\ u_2(x, y, z, t) = 0 \\ u_3(x, y, z, t) = w(x, t) \end{cases} \quad (4b)$$

By assuming large deformation of the imperfect FG-SWBNT micro-composite beam, the nonzero component of the von-Karman strain is approximately expressed as (Wang *et al.* 2015, Wang *et al.* 2013, Gu *et al.* 2019)

$$\begin{aligned} \epsilon_{xx} &= \frac{\partial u}{\partial x} + z \frac{\partial \psi}{\partial x} + \frac{1}{2} \left(\frac{\partial w}{\partial x}\right)^2 + \frac{\partial w}{\partial x} \frac{\partial w_0}{\partial x} \\ \epsilon_{xz} &= \frac{1}{2} \left(\frac{\partial w}{\partial x} + \psi\right), \quad \gamma_{xz} = 2\epsilon_{xz} \end{aligned} \quad (5)$$

where  $w_0$  is the initial geometrical imperfection. For imperfect beams, the initial geometrical imperfection  $w_0$  is assumed to be of the form similar to the deformed shape with  $w$ , and have  $w_0 = \mu w$ ,  $\mu$  is the imperfection parameter.

According to Kelvin–Voigt at real life, micro mechanical properties depend on the time variation. Therefore, visco-elastic model, Young’s modulus  $E$  and shear modulus  $G$  are replaced with the operator (Ghorbanpour Arani *et al.* 2014)

$$E_{visco-elastic} = E \left( 1 + g \frac{\partial}{\partial t} \right) \tag{6}$$

$$G_{visco-elastic} = G \left( 1 + g \frac{\partial}{\partial t} \right)$$

where  $g$  is damping coefficient.

The constitutive equations of electro-thermo-mechanical beam model based on piezo-elasticity theory with considering Kelvin–Voigt model can be written as follows (Ghorbanpour Arani *et al.* 2011 and 2014)

$$\{ \sigma_{ij} \} = (1 + g \frac{\partial}{\partial t}) [ Q_{ijkl} ] \{ \epsilon_{kl} \} - [ e_{kij} ]^T \{ E_k \} - \{ \lambda_{ij} \} T \tag{7}$$

$$\{ D_m \} = [ e_{mkl} ] \{ \epsilon_{kl} \} + [ \epsilon_{mk} ]^T \{ E_k \} + \{ \lambda'_i \} T$$

where  $\sigma_{ij}$  and  $\epsilon_{kl}$  denote the stress and strain tensors, respectively.  $E_k$  and  $c$  are the electric field and electric displacement vectors, respectively.  $c_{ijkl}$ ,  $e_{kij}$ ,  $\lambda_{ij}$ ,  $\epsilon_{mk}$  and  $\lambda'_i$  state the elastic constants, piezoelectric coefficients, thermal expansion coefficients, dielectric, and piezoelectric, respectively. Then, using Hook’s law, stress-strain relations can be stated as follows

$$\begin{Bmatrix} \sigma_{xx} \\ \sigma_{yy} \\ \sigma_{zz} \\ \sigma_{yz} \\ \sigma_{zx} \\ \sigma_{xy} \end{Bmatrix} = \begin{bmatrix} Q_{11} & Q_{12} & Q_{13} & 0 & 0 & 0 \\ Q_{21} & Q_{22} & Q_{23} & 0 & 0 & 0 \\ Q_{31} & Q_{32} & Q_{33} & 0 & 0 & 0 \\ 0 & 0 & 0 & Q_{44} & 0 & 0 \\ 0 & 0 & 0 & 0 & Q_{55} & 0 \\ 0 & 0 & 0 & 0 & 0 & Q_{66} \end{bmatrix} \left( 1 + g \frac{\partial}{\partial t} \right) \begin{Bmatrix} \epsilon_{xx} \\ \epsilon_{yy} \\ \epsilon_{zz} \\ \gamma_{yz} \\ \gamma_{zx} \\ \gamma_{xy} \end{Bmatrix} + \begin{bmatrix} \alpha_x \\ 0 \\ 0 \\ 0 \\ 0 \\ 0 \end{bmatrix} \Delta T - \begin{bmatrix} e_{11} & 0 & 0 \\ e_{12} & 0 & 0 \\ 0 & 0 & 0 \\ 0 & 0 & 0 \\ 0 & 0 & 0 \\ 0 & 0 & 0 \end{bmatrix} \begin{Bmatrix} E_x \\ 0 \\ 0 \end{Bmatrix} \tag{8}$$

where  $E_x$  is the electric field in the  $x$  direction. The electric field versus the electric potential and  $Q_{ij}$  is defined as follows (Ghorbanpour Arani *et al.* 2011)

$$E_x = - \frac{\partial \phi}{\partial x} \tag{9}$$

$$Q_{11} = Q_{22} = Q_{33} = \frac{E_{11}(z)}{1 - \nu_{12}(z) \nu_{21}(z)}$$

$$Q_{12} = Q_{13} = Q_{23} = \frac{\nu_{12}(z) E_{11}(z)}{1 - \nu_{12}(z) \nu_{21}(z)} \tag{10}$$

$$Q_{44} = Q_{55} = Q_{66} = G_{12}(z)$$

The governing equations of micro composite viscoelastic Timoshenko beam based on minimum potential energy principle are obtained as follows:

$$\delta \Pi = 0 \Rightarrow \int_0^t (\delta U^s - \delta T + \delta W_{Ext}) dt = 0 \tag{11}$$

where  $\delta U^s$ ,  $\delta W_{Ext}$ , and  $\delta T$  are the virtual strain energy, the virtual work done by external forces, and the virtual kinetic energy, respectively. The variation of kinetic energy can be written as follows

$$\begin{aligned} \delta \int_0^t T dt &= \int_0^t \int_0^L \rho(z) \left[ \frac{\partial^2 (u + z\psi)^2}{\partial t^2} \delta(u + z\psi) + \left( \frac{\partial^2 w}{\partial t^2} \right) \delta w \right] dx dt \\ &= \int_0^t \int_0^L \rho(z) \left\{ \frac{\partial^2 u}{\partial t^2} \delta u + z \frac{\partial^2 \psi}{\partial t^2} \delta \psi + z \frac{\partial^2 \psi}{\partial t^2} \delta u + z^2 \frac{\partial^2 \psi}{\partial t^2} \delta \psi + \frac{\partial^2 w}{\partial t^2} \delta w \right\} dx dt \tag{12} \\ &\Rightarrow \delta \int_0^t T dt = \int_0^t \int_0^L \left\{ I_0 \frac{\partial^2 u}{\partial t^2} \delta u + I_1 \frac{\partial^2 u}{\partial t^2} \delta \psi + I_1 \frac{\partial^2 \psi}{\partial t^2} \delta u + I_2 \frac{\partial^2 \psi}{\partial t^2} \delta \psi + I_0 \frac{\partial^2 w}{\partial t^2} \delta w \right\} dx dt \end{aligned}$$

The governing electro-dynamics Maxwell equations are written as follows

$$h = \text{Curl}(U \times H) = \nabla \times \begin{vmatrix} u & 0 & w \\ H_x & 0 & 0 \end{vmatrix} = \left( 0, 0, \frac{\partial}{\partial x} w H_x \right)$$

$$f = \mu_1 \times (J \times h) = \mu_1 \times \begin{vmatrix} 0 & -\frac{\partial}{\partial x} \left( \frac{\partial}{\partial x} w H_x \right) & 0 \\ H_x & 0 & 0 \end{vmatrix} \tag{13}$$

$$= \left( 0, 0, \mu_1 H_x^2 \frac{\partial}{\partial x} \left( \frac{\partial w}{\partial x} \right) \right) = \left( 0, 0, \mu_1 H_x^2 \frac{\partial^2 w}{\partial x^2} \right)$$

where  $H$  is magnetic field vector and  $\mu_1$  is the magnetic field permeability. The work done due to the external load such as the elastic medium, axial force, magnetic field, and distributed transverse load for micro-composite beam is described by (Yas and Samadi 2012)

$$W_{Ext} = W_E + W_A + W_L + W_d$$

$$\begin{cases} W_E = - \int_A (F_E w) dA = - \frac{1}{2} \int_A \left( -k_w w + k_g \frac{\partial^2 w}{\partial x^2} \right) w dA \\ W_A = - \frac{1}{2} \int_A P_M \left( \frac{\partial w}{\partial x} \right)^2 dA \\ W_L = - \frac{1}{2} \int_A f_z w dA \\ W_d = - \frac{1}{2} \int_A q w dA \end{cases} \tag{14}$$

The virtual work done by the forces applied on the micro-composite beam can be expressed as

$$\delta W_{Ext} = - \left[ b \int_A \left( -k_w w + k_g \frac{\partial^2 w}{\partial x^2} \right) \delta w dx + \int_A P_M \left( \frac{\partial \delta w}{\partial x} \right) \left( \frac{\partial w}{\partial x} \right) dA + \int_A f_z \delta w dA + \int_A q \delta w dA + \sum_i Q_i^e \delta \Delta_i^e \right] \tag{15}$$

where  $q$ ,  $Q_i^e$ , and  $\Delta_i^e$  are the distributed transverse load, the element generalized forces, and element generalized displacements, respectively (Reddy 2004).

According to the MSGT (Karami and Janghorban 2018, Lam *et al.* 2003), the strain energy  $U^s$  for micro-composite beam reinforced by various distributions of BNNT with initial geometrical imperfection is written as follows

$$U^s = \frac{1}{2} \int_0^L (\epsilon_{ij} \sigma_{ij} + p_i \gamma_i + \tau_{ijk}^{(1)} \eta_{ijk}^{(1)} + m_{ij}^s \chi_{ij}^s) dV \tag{16}$$

Based on the MSGT, the dilatation gradient,  $\gamma_i$ , deviatoric stretch gradient,  $\eta_{ijk}^{(1)}$ , and symmetric rotation gradient tensors,  $\chi_{ij}$ , are defined as:

$$\epsilon_{ij} = \frac{1}{2} (u_{i,j} + u_{j,i})$$

$$\gamma_i = \epsilon_{nm,i}$$

$$\eta_{ijk}^{(1)} = \frac{1}{3} (\epsilon_{jk,i} + \epsilon_{ki,j} + \epsilon_{ij,k}) - \frac{1}{15} (\epsilon_{mn,k} + 2\epsilon_{mk,m}) - \frac{1}{15} [\delta_{jk} (\epsilon_{mn,i} + 2\epsilon_{mi,m}) + \delta_{ki} (\epsilon_{mn,j} + 2\epsilon_{mj,m})] \tag{17}$$

$$\chi_{ij} = \frac{1}{2} \left( \frac{\partial \theta_i}{\partial x_j} + \frac{\partial \theta_j}{\partial x_i} \right), \quad i, j = 1, 2, 3$$

According to the constitutive equations for micro-composite beam reinforced by various distributions of BNNT, the higher order stresses based on MSGT are considered as follows:

$$\begin{aligned} p_i &= 2\mu' l_0^2 \gamma_i \\ \tau_{ijk}^{(1)} &= 2\mu' l_1^2 \eta_{ijk}^{(1)} \\ m_{ij}^s &= 2\mu' l_2^2 \chi_{ij}^s \end{aligned} \quad (18)$$

where  $l_0$ ,  $l_1$  and  $l_2$  are three material length scale parameters. Moreover, the parameters  $p_i$ ,  $\tau_{ijk}^{(1)}$ , and  $m_{ij}$  represent the higher-order stresses; Also  $\mu'$  is shear modulus. Substituting Eq. (4) and (5) into Eqs. (17), the non-zero components of the dilation gradient vector, the deviatoric stretch gradient tensor, the symmetric part of the rotation gradient tensor are obtained. We use the principle of virtual displacements to develop the necessary weak statements of the TBT. The variation of strain energy based on MSGT can be obtained as follows:

$$\begin{aligned} \delta U' &= \int_0^L \left\{ -N_x \delta u + \left( p_{xx}^s + \frac{2}{5} r_{xx}^s - \frac{3}{5} r_{xx}^s - \frac{3}{5} r_{xx}^s \right) \delta u - M_{xx} \delta w + \left( -\frac{1}{2} Y_{xx} - \frac{1}{5} r_{xx}^s + \frac{4}{5} r_{xx}^s - \frac{1}{5} r_{xx}^s \right) \delta w \right. \\ &+ M_{xx} \delta \psi - \left( M_{xx} + p_{xx}^s + \frac{1}{2} Y_{xx} - \frac{2}{5} r_{xx}^s + \frac{8}{5} r_{xx}^s - \frac{2}{5} r_{xx}^s \right) \delta \psi + \left( p_{xx}^s + \frac{2}{5} r_{xx}^s - \frac{3}{5} r_{xx}^s - \frac{3}{5} r_{xx}^s \right) \delta \psi \\ &\left. - \left( \mu + \frac{1}{2} \right) \frac{d}{dx} (N_x w_x) \delta w + (2\mu + 1) \left( p_{xx}^s + \frac{2}{5} r_{xx}^s - \frac{3}{5} r_{xx}^s - \frac{3}{5} r_{xx}^s \right) [-w_{,xx} + w_{,xx}] \delta w \right. \\ &\left. + D_x^i \delta \varphi_i \right\} dx \end{aligned} \quad (19)$$

where

$$\begin{aligned} \{N_x, M_x\} &= \int_A \sigma_{xx}(1, z) dA, \quad M_{xx} = k_s \int_A \sigma_{xx} dA \\ \tau_{xxx}^i &= \int_A z^i \tau_{xxx}^{(1)} dA, \quad \tau_{xxz}^i = \int_A z^i \tau_{xxz}^{(1)} dA, \quad \tau_{xyy}^i = \int_A z^i \tau_{xyy}^{(1)} dA \\ \tau_{xzz}^i &= \int_A z^i \tau_{xzz}^{(1)} dA, \quad \tau_{yyz}^i = \int_A z^i \tau_{yyz}^{(1)} dA, \quad \tau_{zzz}^i = \int_A z^i \tau_{zzz}^{(1)} dA \\ p_{xxx}^i &= \int_A z^i p_{xxx} dA, \quad p_{xxz}^i = \int_A z^i p_{xxz} dA, \quad Y_{xy}^i = \int_A z^i m_{xy}^s dA \end{aligned} \quad (20)$$

Substituting Eq. (20) into Eq. (19), the variation of strain energy for MSGT micro-composite beam reinforced by FG-SWBNTs subjected to electro-mechanical loadings are obtained as follows:

$$\begin{aligned} \delta U' &= \int_0^L \left\{ \frac{\partial \delta u}{\partial x} \left[ \left( 1 + g \frac{\partial}{\partial t} \right) \left[ A_{11}^0 \frac{\partial u}{\partial x} + A_{11}^1 \frac{\partial \psi}{\partial x} + A_{11}^2 \left( \mu + \frac{1}{2} \right) \left( \frac{\partial w}{\partial x} \right)^2 \right] + m_0 \frac{\partial \varphi}{\partial x} \right\} \right. \\ &+ \frac{\partial^2 \delta u}{\partial x^2} \left\{ (2l_0^2 + \frac{4}{5} l_1^2) D_{11}^0 \frac{\partial^2 u}{\partial x^2} + (2l_0^2 + \frac{4}{5} l_1^2) D_{11}^1 \frac{\partial^2 \psi}{\partial x^2} + (2l_0^2 + \frac{4}{5} l_1^2) (2\mu + 1) D_{11}^0 \frac{\partial^2 w}{\partial x^2} \right\} \\ &+ \frac{\partial \delta w}{\partial x} \left\{ k B_{11}^0 \left( 1 + g \frac{\partial}{\partial t} \right) \left[ \psi + \frac{\partial w}{\partial x} \right] + \frac{\partial^2 \delta w}{\partial x^2} \left[ \left( \frac{8}{15} l_1^2 + \frac{1}{4} l_2^2 \right) D_{11}^0 \frac{\partial^2 w}{\partial x^2} + \left( \frac{16}{15} l_1^2 - \frac{1}{4} l_2^2 \right) D_{11}^1 \frac{\partial^2 \psi}{\partial x^2} \right] \right\} \\ &+ \delta \psi \left\{ k B_{11}^0 \left( 1 + g \frac{\partial}{\partial t} \right) \left[ \psi + \frac{\partial w}{\partial x} \right] + \frac{\partial \delta \psi}{\partial x} \left[ \left( 1 + g \frac{\partial}{\partial t} \right) \left[ A_{11}^0 \frac{\partial u}{\partial x} + A_{11}^1 \frac{\partial \psi}{\partial x} + A_{11}^2 \left( \mu + \frac{1}{2} \right) \left( \frac{\partial w}{\partial x} \right)^2 \right] \right. \right. \\ &+ m_1 \frac{\partial \varphi}{\partial x} + (2l_0^2 + \frac{32}{15} l_1^2 + \frac{1}{4} l_2^2) D_{11}^0 \frac{\partial \psi}{\partial x} + \left. \left. \left( \frac{16}{15} l_1^2 - \frac{1}{4} l_2^2 \right) D_{11}^1 \frac{\partial^2 w}{\partial x^2} \right] \right\} \\ &+ \frac{\partial^2 \delta \psi}{\partial x^2} \left\{ (2l_0^2 + \frac{4}{5} l_1^2) D_{11}^0 \frac{\partial^2 u}{\partial x^2} + (2l_0^2 + \frac{4}{5} l_1^2) D_{11}^1 \frac{\partial^2 \psi}{\partial x^2} + (2l_0^2 + \frac{4}{5} l_1^2) (2\mu + 1) D_{11}^0 \frac{\partial^2 w}{\partial x^2} \right\} \\ &+ 2(\mu + \frac{1}{2}) \frac{\partial \delta w}{\partial x} \frac{\partial w}{\partial x} \left\{ \left( 1 + g \frac{\partial}{\partial t} \right) \left[ A_{11}^0 \frac{\partial u}{\partial x} + A_{11}^1 \frac{\partial \psi}{\partial x} + A_{11}^2 \left( \mu + \frac{1}{2} \right) \left( \frac{\partial w}{\partial x} \right)^2 \right] + m_2 \frac{\partial \varphi}{\partial x} \right\} \\ &+ (2\mu + 1) \left[ \frac{\partial^2 \delta w}{\partial x^2} \frac{\partial w}{\partial x} + \frac{\partial \delta w}{\partial x} \frac{\partial^2 w}{\partial x^2} \right] \left\{ (2l_0^2 + \frac{4}{5} l_1^2) D_{11}^0 \frac{\partial^2 u}{\partial x^2} + (2l_0^2 + \frac{4}{5} l_1^2) D_{11}^1 \frac{\partial^2 \psi}{\partial x^2} + \right. \\ &\left. + (2l_0^2 + \frac{4}{5} l_1^2) (2\mu + 1) D_{11}^0 \frac{\partial^2 w}{\partial x^2} \right\} + \frac{\partial \delta \varphi}{\partial x} \left\{ m_0 \frac{\partial u}{\partial x} + m_1 \frac{\partial \psi}{\partial x} + m_2 \left( \mu + \frac{1}{2} \right) \left( \frac{\partial w}{\partial x} \right)^2 - m_2 \frac{\partial \varphi}{\partial x} \right\} dx \end{aligned} \quad (21)$$

Using Eq. (21) and separation of variables, for the nonlinear bending, buckling and free vibration analysis of micro-composite beams, a weak form may be derived from

the dynamic form of the virtual work principle under the assumptions of the TBT reinforced by FG-SWBNTs based on MSGT are obtained as follows:

$$\begin{aligned} &\left\{ \int_0^L \left[ A_{11}^0 \frac{\partial \delta u}{\partial x} \frac{\partial u}{\partial x} dx + \left( 2l_0^2 + \frac{4}{5} l_1^2 \right) D_{11}^0 \frac{\partial^2 \delta u}{\partial x^2} \frac{\partial^2 u}{\partial x^2} dx + \int_0^L A_{11}^2 \left( \mu + \frac{1}{2} \right) \frac{\partial \delta u}{\partial x} \left( \frac{\partial w}{\partial x} \right)^2 dx \right. \right. \\ &+ \left. \left. \int_0^L \left( 2l_0^2 + \frac{4}{5} l_1^2 \right) (2\mu + 1) D_{11}^0 \frac{\partial^2 \delta u}{\partial x^2} \frac{\partial^2 w}{\partial x^2} \frac{\partial w}{\partial x} dx + \int_0^L A_{11}^1 \frac{\partial \delta u}{\partial x} \frac{\partial \psi}{\partial x} dx \right. \right. \\ &+ \left. \left. \int_0^L \left( 2l_0^2 + \frac{4}{5} l_1^2 \right) D_{11}^1 \frac{\partial^2 \delta u}{\partial x^2} \frac{\partial^2 \psi}{\partial x^2} dx + \int_0^L m_0 \frac{\partial \delta u}{\partial x} \frac{\partial \varphi}{\partial x} dx \right. \right. \\ &\left. \left. \int_0^L g A_{11}^2 \frac{\partial \delta u}{\partial x} \frac{\partial^2 w}{\partial x^2} dx + 2 \int_0^L g A_{11}^2 \left( \mu + \frac{1}{2} \right) \frac{\partial \delta u}{\partial x} \frac{\partial w}{\partial x} \frac{\partial^2 w}{\partial x^2} dx + \int_0^L g A_{11}^2 \frac{\partial \delta u}{\partial x} \frac{\partial^2 \psi}{\partial x^2} dx \right\} - \right. \\ &\left. \left\{ \int_0^L I_x \delta u \frac{\partial^2 u}{\partial t^2} dx + \int_0^L I_x \delta u \frac{\partial^2 \psi}{\partial t^2} dx \right\} - Q_x^i \delta u(x_i) - Q_x^i \delta u(x_i) = 0 \end{aligned} \quad (22-a)$$

$$\begin{aligned} &\left\{ b \int_0^L k \delta w w dx - b \int_0^L k \delta w \frac{\partial w}{\partial x} dx + \int_0^L k B_{11}^0 \frac{\partial \delta w}{\partial x} \frac{\partial w}{\partial x} dx + \int_0^L \left( \frac{8}{15} l_1^2 + \frac{1}{4} l_2^2 \right) D_{11}^0 \frac{\partial^2 \delta w}{\partial x^2} \frac{\partial^2 w}{\partial x^2} dx + \right. \\ &\left. \int_0^L \left( \frac{16}{15} l_1^2 - \frac{1}{4} l_2^2 \right) D_{11}^1 \frac{\partial^2 \delta w}{\partial x^2} \frac{\partial^2 \psi}{\partial x^2} dx + \int_0^L k B_{11}^1 \frac{\partial \delta w}{\partial x} \psi dx + 2 \int_0^L \left( \mu + \frac{1}{2} \right) A_{11}^2 \frac{\partial \delta w}{\partial x} \frac{\partial u}{\partial x} \frac{\partial w}{\partial x} dx + \right. \\ &+ 2 \int_0^L \left( \mu + \frac{1}{2} \right) A_{11}^2 \frac{\partial \delta w}{\partial x} \frac{\partial \psi}{\partial x} \frac{\partial w}{\partial x} dx + 2 \int_0^L \left( \mu + \frac{1}{2} \right) A_{11}^2 \frac{\partial \delta w}{\partial x} \left( \frac{\partial w}{\partial x} \right)^2 \frac{\partial w}{\partial x} dx + 2 \int_0^L \left( \mu + \frac{1}{2} \right) m_2 \frac{\partial \delta w}{\partial x} \frac{\partial \varphi}{\partial x} \frac{\partial w}{\partial x} dx \\ &+ \left. \int_0^L (2\mu + 1) \left( 2l_0^2 + \frac{4}{5} l_1^2 \right) D_{11}^0 \frac{\partial^2 \delta w}{\partial x^2} \frac{\partial^2 w}{\partial x^2} \frac{\partial w}{\partial x} dx + \int_0^L (2\mu + 1) \left( 2l_0^2 + \frac{4}{5} l_1^2 \right) D_{11}^1 \frac{\partial^2 \delta w}{\partial x^2} \frac{\partial^2 \psi}{\partial x^2} \frac{\partial w}{\partial x} dx + \right. \\ &\left. \int_0^L (2\mu + 1) \left( 2l_0^2 + \frac{4}{5} l_1^2 \right) D_{11}^0 \frac{\partial^2 \delta w}{\partial x^2} \frac{\partial^2 w}{\partial x^2} \frac{\partial^2 w}{\partial x^2} dx + \int_0^L (2\mu + 1) \left( 2l_0^2 + \frac{4}{5} l_1^2 \right) D_{11}^1 \frac{\partial^2 \delta w}{\partial x^2} \frac{\partial^2 \psi}{\partial x^2} \frac{\partial^2 w}{\partial x^2} dx + \right. \\ &\left. \int_0^L (2\mu + 1) \left( 2l_0^2 + \frac{4}{5} l_1^2 \right) D_{11}^0 \frac{\partial^2 \delta w}{\partial x^2} \frac{\partial^2 \psi}{\partial x^2} \frac{\partial^2 w}{\partial x^2} dx + \int_0^L (2\mu + 1) \left( 2l_0^2 + \frac{4}{5} l_1^2 \right) D_{11}^1 \frac{\partial^2 \delta w}{\partial x^2} \left( \frac{\partial w}{\partial x} \right)^2 \frac{\partial^2 w}{\partial x^2} dx \right. \\ &+ \left. \int_0^L k B_{11}^2 \frac{\partial \delta w}{\partial x} \frac{\partial w}{\partial x} dx + \int_0^L k B_{11}^2 \frac{\partial \delta w}{\partial x} \frac{\partial \psi}{\partial x} dx + 2 \int_0^L \left( \mu + \frac{1}{2} \right) g A_{11}^2 \frac{\partial \delta w}{\partial x} \frac{\partial u}{\partial x} \frac{\partial w}{\partial x} dx + \right. \\ &+ \left. 2 \int_0^L \left( \mu + \frac{1}{2} \right) g A_{11}^2 \frac{\partial \delta w}{\partial x} \frac{\partial \psi}{\partial x} \frac{\partial w}{\partial x} dx + 4 \int_0^L \left( \mu + \frac{1}{2} \right) g A_{11}^2 \frac{\partial \delta w}{\partial x} \frac{\partial w}{\partial x} \frac{\partial w}{\partial x} dx \right. \\ &\left. - \int_0^L I_x \delta w \frac{\partial^2 w}{\partial t^2} dx - \int_0^L \left[ p_w \frac{\partial \delta w}{\partial x} \frac{\partial w}{\partial x} \right] dx - \int_0^L \left[ q \delta w w \right] dx - Q_x^i \delta w(x_i) - Q_x^i \delta w(x_i) = 0 \end{aligned} \quad (22-b)$$

$$\begin{aligned} &\left\{ \int_0^L \left[ A_{11}^1 \frac{\partial \delta \psi}{\partial x} \frac{\partial u}{\partial x} dx + \left( 2l_0^2 + \frac{4}{5} l_1^2 \right) D_{11}^1 \frac{\partial^2 \delta \psi}{\partial x^2} \frac{\partial^2 u}{\partial x^2} dx \right. \right. \\ &+ \left. \left. \int_0^L k B_{11}^0 \delta \psi \frac{\partial w}{\partial x} dx + \int_0^L \left( \frac{16}{15} l_1^2 - \frac{1}{4} l_2^2 \right) D_{11}^1 \frac{\partial^2 \delta \psi}{\partial x^2} \frac{\partial^2 w}{\partial x^2} dx \right. \right. \\ &+ \left. \left. \int_0^L k B_{11}^0 \delta \psi \psi dx + \int_0^L A_{11}^1 \frac{\partial \delta \psi}{\partial x} \frac{\partial \psi}{\partial x} dx + \int_0^L \left( 2l_0^2 + \frac{32}{15} l_1^2 + \frac{1}{4} l_2^2 \right) D_{11}^0 \frac{\partial^2 \delta \psi}{\partial x^2} \frac{\partial^2 \psi}{\partial x^2} dx \right. \right. \\ &+ \left. \left. \int_0^L \left( 2l_0^2 + \frac{4}{5} l_1^2 \right) D_{11}^1 \frac{\partial^2 \delta \psi}{\partial x^2} \frac{\partial^2 \psi}{\partial x^2} dx + \int_0^L m_1 \frac{\partial \delta \psi}{\partial x} \frac{\partial \varphi}{\partial x} dx + \int_0^L A_{11}^2 \left( \mu + \frac{1}{2} \right) \frac{\partial \delta \psi}{\partial x} \left( \frac{\partial w}{\partial x} \right)^2 dx \right. \right. \\ &+ \left. \left. \int_0^L \left( 2l_0^2 + \frac{4}{5} l_1^2 \right) (2\mu + 1) D_{11}^1 \frac{\partial^2 \delta \psi}{\partial x^2} \frac{\partial^2 w}{\partial x^2} \frac{\partial w}{\partial x} dx \right. \right. \\ &\left. \left. \int_0^L k B_{11}^2 \delta \psi \frac{\partial w}{\partial x} dx + \int_0^L k B_{11}^2 \delta \psi \frac{\partial \psi}{\partial x} dx + \int_0^L A_{11}^2 g \frac{\partial \delta \psi}{\partial x} \frac{\partial^2 u}{\partial x^2} dx \right. \right. \\ &+ \left. \left. \int_0^L A_{11}^2 g \frac{\partial \delta \psi}{\partial x} \frac{\partial^2 \psi}{\partial x^2} dx + 2 \int_0^L \left( \mu + \frac{1}{2} \right) A_{11}^2 g \frac{\partial \delta \psi}{\partial x} \frac{\partial w}{\partial x} \frac{\partial w}{\partial x} dx \right. \right. \\ &\left. \left. - \int_0^L I_x \delta \psi \frac{\partial^2 u}{\partial t^2} dx + \int_0^L I_x \delta \psi \frac{\partial^2 \psi}{\partial t^2} dx \right\} - Q_x^i \delta \psi(x_i) - Q_x^i \delta \psi(x_i) = 0 \end{aligned} \quad (22-c)$$

$$\left\{ \int_0^L m_0 \frac{\partial \delta \varphi}{\partial x} \frac{\partial u}{\partial x} dx + \int_0^L m_1 \frac{\partial \delta \varphi}{\partial x} \frac{\partial \psi}{\partial x} dx - \int_0^L m_2 \frac{\partial \delta \varphi}{\partial x} \frac{\partial \varphi}{\partial x} dx + \int_0^L \left( \mu + \frac{1}{2} \right) m_0 \frac{\partial \delta \varphi}{\partial x} \left( \frac{\partial w}{\partial x} \right)^2 dx \right\} = 0 \quad (22-d)$$

where

$$\begin{aligned} A_{11}^i &= b \int_{-\frac{h}{2}}^{\frac{h}{2}} z^i c_{11} dz, \quad i = 0, 1, 2, \\ B_{11}^i &= D_{11}^i = b \int_{-\frac{h}{2}}^{\frac{h}{2}} z^i G dz, \quad i = 0, 1, 2 \\ \{m_0, m_1\} &= b \int_{-\frac{h}{2}}^{\frac{h}{2}} (1, z) e_{11} dz, \quad m_2 = b \int_{-\frac{h}{2}}^{\frac{h}{2}} \epsilon_{11} dz \end{aligned} \quad (23)$$

## 5. Solving method

In this paper, FEM is used to solve the governing equations of micro-composite beams. According to FEM, the axial displacement  $u$ , transverse deflection  $w$ , rotation  $\psi_x$  and electrical boundary condition  $\varphi$  are interpolated as follows (Chakraborty and Mahaptra 2002, Reddy 2004)

$$\begin{aligned} u(x) &= N_1 u_1 + N_2 w_1 + N_3 \psi_1 + N_4 u_2 + N_5 w_2 + N_6 \psi_2 = [N_u(x)]\{q_u\} \\ w(x) &= N_7 w_1 + N_8 \psi_1 + N_9 w_2 + N_{10} \psi_2 = [N_w(x)]\{q_w\} \\ \psi_x(x) &= N_{11} w_1 + N_{12} \psi_1 + N_{13} w_2 + N_{14} \psi_2 = [N_\psi(x)]\{q_\psi\} \\ \varphi(x) &= N_{15} \varphi_1 + N_{16} \varphi_2 = [N_\varphi(x)]\{q_\varphi\} \end{aligned} \quad (24)$$

where  $N_i$  ( $i=1, \dots, 16$ ) are the associated shape functions for axial, transverse, rotational and electrical degrees of freedom, respectively, that the following steps are considered to find the shape functions.

The interpolation functions of displacement fields for the FE formulation are written as follows (Chakraborty *et al.* 2002)

$$\begin{aligned} u(x) &= c_1 + c_2 x + c_3 x^2 \\ w(x) &= c_4 + c_5 x + c_6 x^2 + c_7 x^3 \\ \psi_x(x) &= c_8 + c_9 x + c_{10} x^2 \\ \varphi(x) &= c_{11} + c_{12} x \end{aligned} \quad (25)$$

Eq. (25) has twelve constants and only eight boundary conditions (four degrees of freedom at each node of the element). The four additional dependent constants can be expressed in terms of eight other independent constants by substituting Eqs. (25) into the governing equations of motion, so we have

$$\begin{aligned} c_7 &= -\frac{1}{3}c_{10}, \quad c_6 = -\frac{1}{2}c_9, \quad c_3 = \left(\frac{-A_{11}}{A_{10}}\right)c_{10}, \\ c_8 &= \frac{(-2A_{11}^2 + 2A_{10}A_{12})c_{10} - (A_{10}B_{10}k_s)c_5}{A_{10}B_{10}k_s} \end{aligned} \quad (26)$$

By substituting Eq. (26) into Eq. (25), the displacement fields are derived as the following form

$$\begin{aligned} u &= c_1 + c_2 x + \left(-\frac{A_{11}}{A_{10}}c_{10}\right)x^2 \\ w &= c_4 + c_5 x + \left(-\frac{1}{2}c_9\right)x^2 + \left(-\frac{1}{3}c_{10}\right)x^3 \\ \psi_x &= -c_5 + c_9 x + \left(\frac{-2A_{11}^2 + 2A_{10}A_{12}}{A_{10}B_{10}k_s} + x^2\right)c_{10} \\ \varphi &= c_{11} + c_{12} x \end{aligned} \quad (27)$$

The equations of FEM displacements for an element of micro-composite beam reinforced by various distributions of BNNs can be expressed as follows (Chakraborty *et al.* 2002, Alimirzaei 2017)

$$\begin{aligned} \{q\} &= \begin{Bmatrix} u \\ w \\ \psi_x \\ \varphi \end{Bmatrix} = \begin{Bmatrix} 1 & x & 0 & 0 & 0 & \left(-\frac{A_{11}}{A_{10}}\right)x^2 & 0 & 0 \\ 0 & 0 & 1 & x & \frac{-x^2}{2} & \frac{-x^3}{3} & 0 & 0 \\ 0 & 0 & 0 & -1 & x & \left(\frac{-2A_{11}^2 + 2A_{10}A_{12}}{A_{10}B_{10}k_s} + x^2\right) & 0 & 0 \\ 0 & 0 & 0 & 0 & 0 & 0 & 1 & x \end{Bmatrix} \begin{Bmatrix} c_1 \\ c_2 \\ c_4 \\ c_5 \\ c_9 \\ c_{10} \\ c_{11} \\ c_{12} \end{Bmatrix} = [N(x)]\{a\} \\ \{a\} &= \{c_1, c_2, c_4, c_5, c_9, c_{10}, c_{11}, c_{12}\}^T \end{aligned} \quad (28)$$

where  $[N(x)]$  is the matrix containing functions of  $x$  and it is of size  $4 \times 8$ . The column vector  $\{a\}$  of independent constants can be expressed in terms of nodal displacements by substituting eight displacement boundary conditions into Eq. (28).

$$\begin{aligned} [G]^{-1} &= \begin{Bmatrix} N(0) \\ N(l_e) \end{Bmatrix}, \quad \{\hat{q}\} = [G]^{-1}\{a\}, \\ \{a\} &= [G]\{\hat{q}\}, \quad l_e = \frac{L}{\text{numerelement}} \end{aligned} \quad (29)$$

Finally, we have

$$\begin{aligned} \{q\} &= \begin{Bmatrix} u(x) \\ w(x) \\ \psi_x(x) \\ \varphi(x) \end{Bmatrix} = [N(x)]\{a\} = [N(x)][G]\{\hat{q}\} = [\bar{N}(x)]\{q\} \\ \bar{N}(x) &= \begin{bmatrix} N_1 & N_2 & N_3 & 0 & N_4 & N_5 & N_6 & 0 \\ 0 & N_7 & N_8 & 0 & 0 & N_9 & N_{10} & 0 \\ 0 & N_{11} & N_{12} & 0 & 0 & N_{13} & N_{14} & 0 \\ 0 & 0 & 0 & N_{15} & 0 & 0 & 0 & N_{16} \end{bmatrix} = \begin{Bmatrix} N_u(x) \\ N_w(x) \\ N_\psi(x) \\ N_\varphi(x) \end{Bmatrix} \end{aligned} \quad (30)$$

Finally, explicit form of shape functions is given in Appendix A.

Using Eq. (24) and  $\delta u(x) = N_{ui}(x)$ ,  $\delta w(x) = N_{wi}(x)$ ,  $\delta \psi(x) = N_{\psi i}(x)$ , and  $\delta \varphi(x) = N_{\varphi i}(x)$  (Reddy 2004) into the weak form equations of micro-composite beam (i.e., (22-a)-(22-d)), respectively, the finite element formulations for the bending, buckling and free vibration analysis can be obtained. Using Eqs. (22) and (28) and separation of variables, the following governing equations of motion for micro-composite beam reinforced by FG-SWBNNs based on MSGT are obtained as follows

$$[M_{ij}]\{\ddot{q}\} + [C_{ij}]\{\dot{q}\} + [k_{ij}]\{q\} + [G_{ij}]\{q\} = \{f_i\} \quad (31)$$

In Eq. (31),  $[K_{ij}]$ ,  $[M_{ij}]$ ,  $[C_{ij}]$  and  $[G_{ij}]$  are the stiffness, mass and damping matrices, respectively which are defined in Appendix B.

### 5.1 Equation of motion

The equation of motion of the whole structure system is represented by

$$\begin{aligned} &\begin{bmatrix} M_{dd} & 0 \\ 0 & 0 \end{bmatrix} \begin{Bmatrix} \ddot{q}_d \\ \ddot{q}_\varphi \end{Bmatrix} + \begin{bmatrix} D_{dd} & 0 \\ 0 & 0 \end{bmatrix} \begin{Bmatrix} \dot{q}_d \\ \dot{q}_\varphi \end{Bmatrix} \\ &+ \underbrace{\begin{bmatrix} K_{dd} & K_{d\varphi} \\ K_{\varphi d} & K_{\varphi\varphi} \end{bmatrix}}_{K_{\text{Nonlinear}} + K_{\text{Linear}}} \begin{Bmatrix} q_d \\ q_\varphi \end{Bmatrix} + \begin{bmatrix} G_{dd} & 0 \\ 0 & 0 \end{bmatrix} \begin{Bmatrix} q_d \\ q_\varphi \end{Bmatrix} = \begin{Bmatrix} f_d \\ f_\varphi \end{Bmatrix} \end{aligned} \quad (32)$$

$\{q_d\}$  is generalized displacements coordinates vector,  $\{q_\varphi\}$  is the generalized electric coordinate's vector describing the applied voltages at the actuators, which Eq. (32) can be expressed as follows:

$$\begin{aligned} & [M_{dd}] \{\ddot{q}_d\} + [D_{dd}] \{\dot{q}_d\} + [K_{dd}] \{q_d\} \\ & + [K_{d\varphi}] \{q_\varphi\} + [G_{dd}] \{q_d\} = \{F_d\} \end{aligned} \quad (33)$$

$$\begin{aligned} & [K_{\varphi d}] \{q_d\} + [K_{\varphi\varphi}] \{q_\varphi\} = \{f_\varphi\} \\ \Rightarrow \{q_\varphi\} &= [K_{\varphi\varphi}^{-1}] (\{f_\varphi\} - [K_{\varphi d}] \{q_d\}) \end{aligned} \quad (34)$$

Substituting Eq. (34) into Eq. (33), the equations of motion can be derived as follows

$$[M_{dd}] \{\ddot{q}_d\} + [D_{dd}] \{\dot{q}_d\} + [K_m] \{q_d\} + [G_{dd}] \{q_d\} = \{F_m\} \quad (35)$$

where

$$\begin{aligned} [K_m] &= [K_{dd}] - [K_{d\varphi}] [K_{\varphi\varphi}^{-1}] [K_{\varphi d}] \\ \{F_m\} &= \{f_d\} - [K_{d\varphi}] [K_{\varphi\varphi}^{-1}] \{f_\varphi\} \end{aligned} \quad (36)$$

➤ For static analysis, the formulation of micro composite Timoshenko beams can be obtained as

$$[K_m] \{q_d\} = \{F_m\} \quad (37)$$

where  $[K_m]$  and  $\{F_m\}$  are stiffness matrix and external distributed load vector, respectively.  $\{q_d\}$  denotes displacement vector which is demonstrated as

$$\begin{aligned} \{q_d\} &= \{u \quad w \quad \psi\}^T \\ &= ([K_{dd}] - [K_{d\varphi}] [K_{\varphi\varphi}^{-1}] [K_{\varphi d}])^{-1} (\{f_d\} - [K_{d\varphi}] [K_{\varphi\varphi}^{-1}] \{f_\varphi\}) \end{aligned} \quad (38)$$

➤ Also the critical buckling load is obtained as the following form

$$([K_m] - P_M [K^s]) \{q_d\} = 0 \quad (39)$$

➤ And, for vibration analysis, it can be rewritten as

$$\begin{aligned} q_d &= q'_d \exp(i\omega t) \\ ([M_{dd}] \omega^2 + [D_{dd}] i \omega + [K_m]) \{q'_d\} &= 0 \end{aligned} \quad (40)$$

For solving the Eq. (40) and reducing it to the standard form of eigenvalue problem, it is convenient to rewrite Eq. (40) as the following first order variable as

$$\begin{aligned} \omega \begin{Bmatrix} q_d \\ \dot{q}_\varphi \end{Bmatrix} &= [A] \begin{Bmatrix} q_d \\ \dot{q}_\varphi \end{Bmatrix}; \\ [A] &= \begin{bmatrix} [0] & [I] \\ -[M_{dd}^{-1}] [D_{dd}] & -[M_{dd}^{-1}] [K_m] \end{bmatrix} \end{aligned} \quad (41)$$

where  $[A]$ ,  $[0]$  and  $[I]$  are the state, zero and unitary matrices, respectively. The results are containing two real

and imaginary parts. The imaginary part is corresponding to the system damping and the real part representing natural frequencies of the system.

## 5.2 Linearization procedure

The linearization process can be accomplished with two type techniques, namely the Picard (direct iteration procedure) or the Newton-Raphson's method. For checking the convergence behaviour of both the methods of linearization's with hp-spectral methods, these methods were implemented. Some of the advantages of the Newton-Raphson method are a faster convergence rate. The linearized problem with the Newton's method is represented as follows (Reddy 2004)

$$[k_1(\{\Delta\}^{(r-1)})] \{\Delta\}^r = -\{R(\{\Delta\}^{(r-1)})\} = \{F\} - ([k^e] \{\Delta^e\})^{(r-1)} \quad (42)$$

where the tangent stiffness matrix  $[k_1]$  associated with the micro-composite beam element is calculated as follows

$$[k_1] = - \left( \frac{\partial \{R\}}{\partial \{\Delta\}} \right)^{(r-1)} \quad (43)$$

The solution at the  $r$ th iteration is then given by:  $\{\Delta\}^r = \{\Delta\}^{(r-1)} + \{\delta\Delta\}^r$ .

For the check of the convergence criterion, it can be computed by using the increment of the solutions vector, i.e.,  $\{\Delta U\}$ , as follows (Reddy 2004)

$$\sqrt{\frac{\sum_{I=1}^N (\Delta U_I)^2}{\sum_{I=1}^N (U_I^{(0)})^2}} < \tilde{\lambda} \quad (44)$$

Alternatively, the objective of the iteration process is to reduce this residual to a very small, negligible value,  $\tilde{\lambda}$

$$\sqrt{\sum_{I=1}^N R_I^2} < \tilde{\lambda} \quad (45)$$

The flow chart for nonlinear bending of micro-composite beams is shown in Fig. 2.

## 6. Numerical results and discussion

The numerical results of nonlinear vibration, buckling and bending of micro-composite beam reinforced by FG-SWBNNs under the distributed load  $q = 10 \mu N/\mu m$  using FEM are presented. Mechanical properties of micro-composite beam are given in Table 1 (Mohammadimehr *et al.* 2016). Also  $\eta_i$  coefficients for different SWBNNs volume fractions are shown in Table 2 (Moradi *et al.* 2013).

All material length scale parameters and the height of micro composite beam ( $h$ ) are considered to be equal to each other as  $l_0 = l_1 = l_2 = h = 17.6 \mu m$ . Moreover, the width of micro composite beam ( $b$ ) and the length of micro composite beam ( $L$ ) are considered  $2h$  and  $20h$ , respectively.

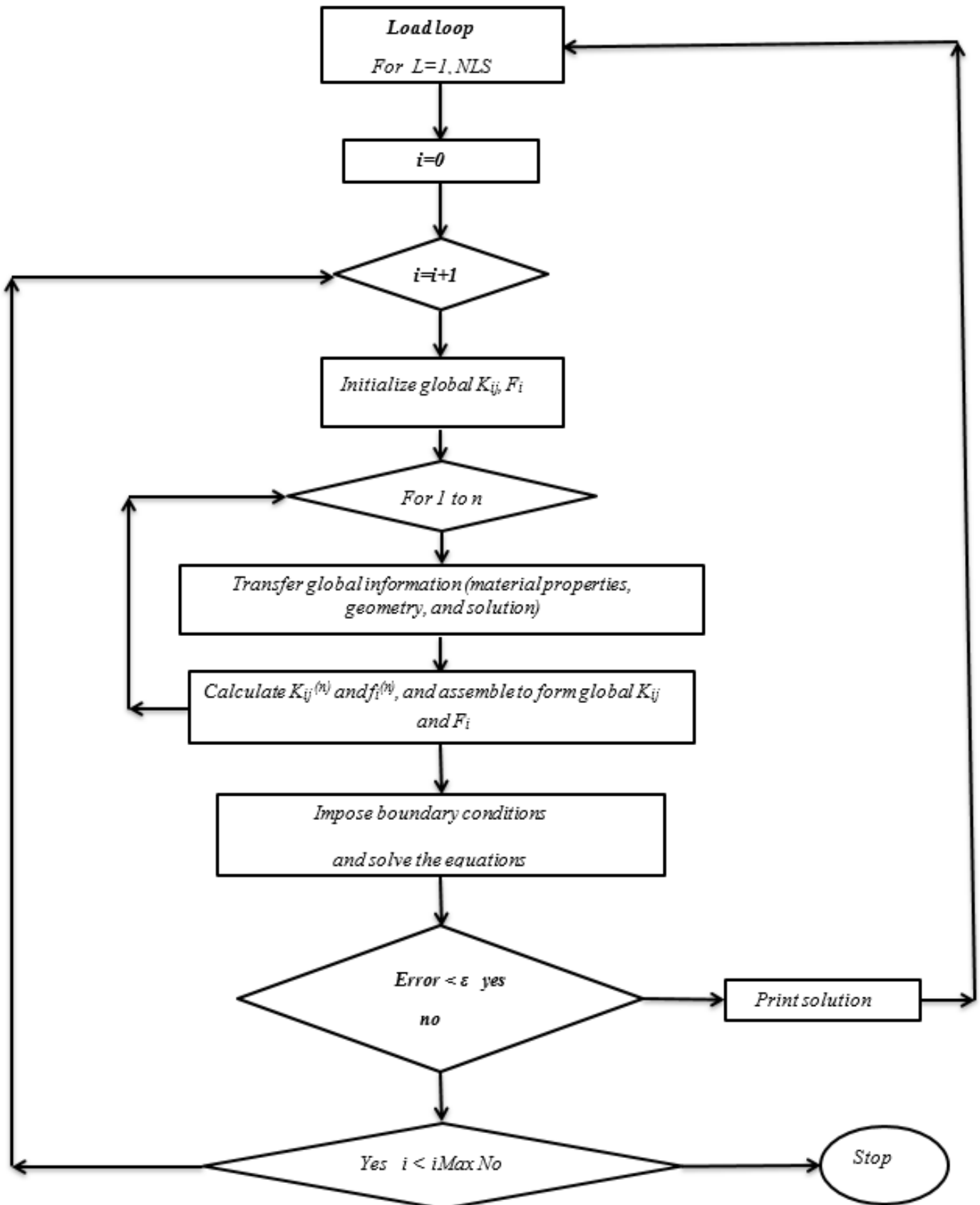


Fig. 2 A computer flowchart of Matlab software for the nonlinear finite element analysis of micro composite Timoshenko beams

Table 1 Material properties of SWBNNTs as reinforcement (Mohammadimehr *et al.* 2016)

$V_{BNNT}^*$	$E_{11}^{BNNT}$ (TPa)	$E_m$ (GPa)	$\rho_{BNNT}$ ( $\frac{kg}{m^3}$ )	$\rho_m$ ( $\frac{kg}{m^3}$ )	$\nu_{BNNT}$	$\nu_m$	$e$ ( $\frac{C}{m^2}$ )	$\epsilon_{11}$
0.17	1.8	3.59	2300	1220	0.34	0.34	0.95	1.1068e-8

Table 2  $\eta_i$  Coefficients of SWBNNTs (Moradi *et al.* 2013)

$V_{BNNT}^*$	$\eta_1$	$\eta_2$	$\eta_3$
0.12	0.137	1.022	0.7154
0.17	0.142	1.626	1.1382
0.28	0.141	1.585	1.1095

Table 3 Dimensionless natural frequency of composite beam using TBT ( $L/h=15$ )

$v_{CNT}^*$	Boundary condition	UD		FG- $\nabla$ (USFG)		FG-X (SFG)	
		Yas and Samadi	Present work	Yas and Samadi	Present work	Yas and Samadi	Present work
0.12	C-C	1.5085	1.506	1.4068	1.4060	1.6000	1.5956
	C-F	0.3764	0.376	0.3193	0.3199	0.4416	0.4415

Table 4 Dimensionless critical buckling load of composite beam using TBT ( $L/h=15$ )

$v_{CNT}^*$	Boundary condition	UD		FG- $\nabla$ (USFG)		FG-X (SFG)	
		Yas and Samadi	Present work	Yas and Samadi	Present work	Yas and Samadi	Present work
0.12	C-C	0.21395	0.21153	0.1819	0.1848	0.24593	0.24106
	C-F	0.03124	0.03522	0.0220	0.0203	0.04435	0.04913

Table 5 Deflections of beam using (EBT) with  $L/h=100$  and  $q = 1N/m$

Boundary condition	Exact solution	Present work
C-C	0.10417	0.10420
S-S	0.52083	0.52080

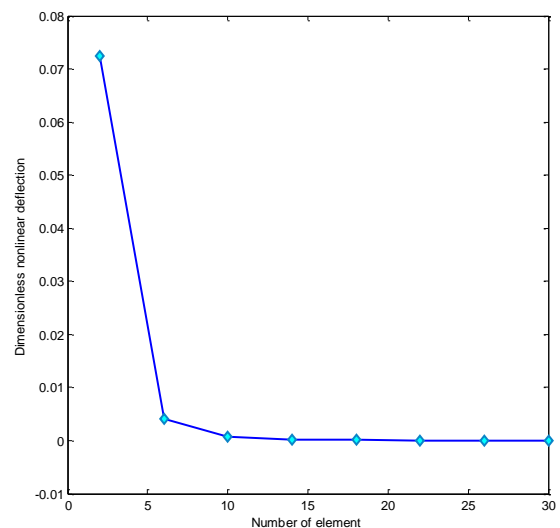
The obtained results for beam are compared with the obtained results by Yas and Samadi (2002). These results are listed in Tables 3-5. A good agreement is observed between FEM results (present work) and the obtained results by the other researchers.

**6.1 Bending and buckling of the micro-composite beam reinforced by FG-SWBNNTs**

Figs. 3(a) and (b) show the convergence of the non-dimensional nonlinear deflection and critical buckling load with the number of elements for micro-composite beam. The obtained results prove the convergence of the predicted results of the present finite element model. It is observed from these figures that the number of elements required for convergence of the micro composite beam is equal to 10 and 40 elements, respectively.

Figs. 4(a) and (b) indicate the number of repeat procedures and error to achieve the convergence of micro-composite beams. As can be seen from this curve, two different methods are used to examine the convergence of systems and both methods eventually converge to a point.

According to this figure with increasing distribution transverse load of micro-composite beam, the number of iterations for convergence system increases.



(a)

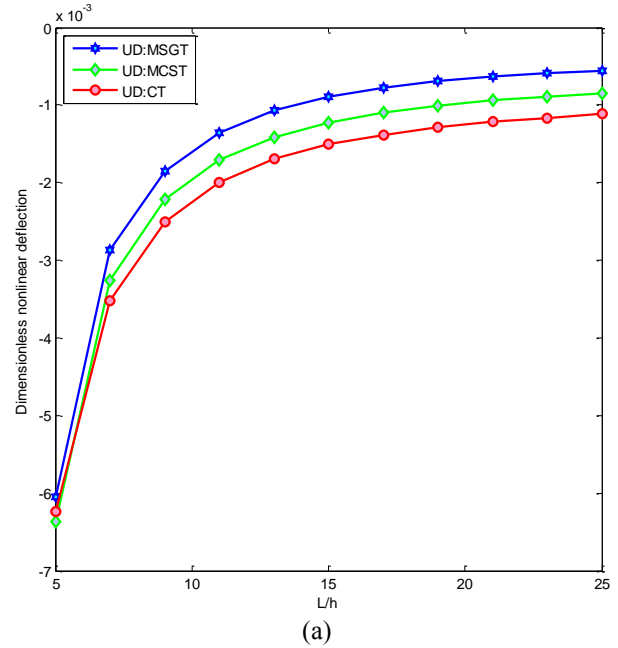
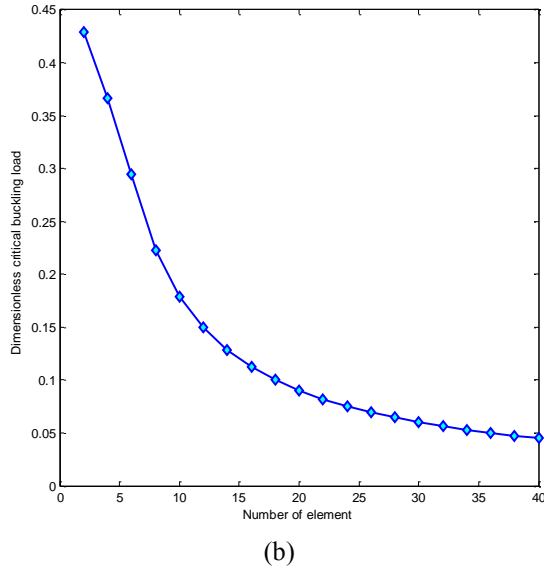


Fig. 3 Number of elements for smart micro composite beam for a) Dimensionless nonlinear deflection b) Dimensionless critical buckling load

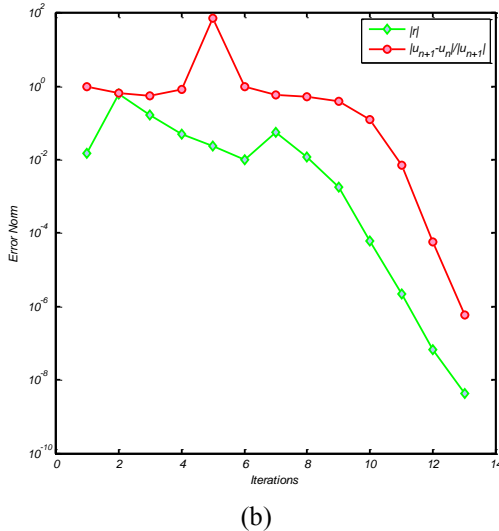
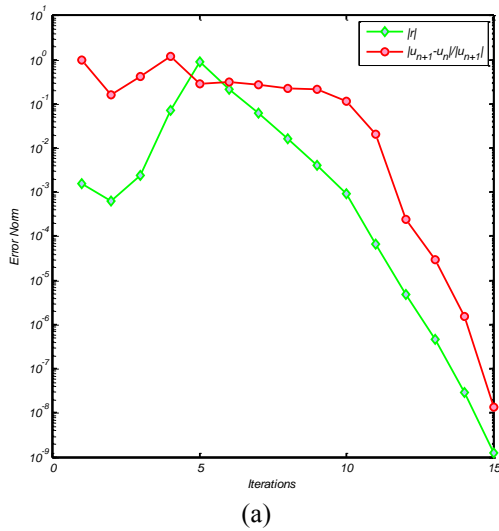


Fig. 4 Error norm of FEM solution for nonlinear micro composite beam under distributed transverse load for a)  $q = 100 \frac{\mu N}{\mu m}$ , b)  $q = 10 \frac{\mu N}{\mu m}$

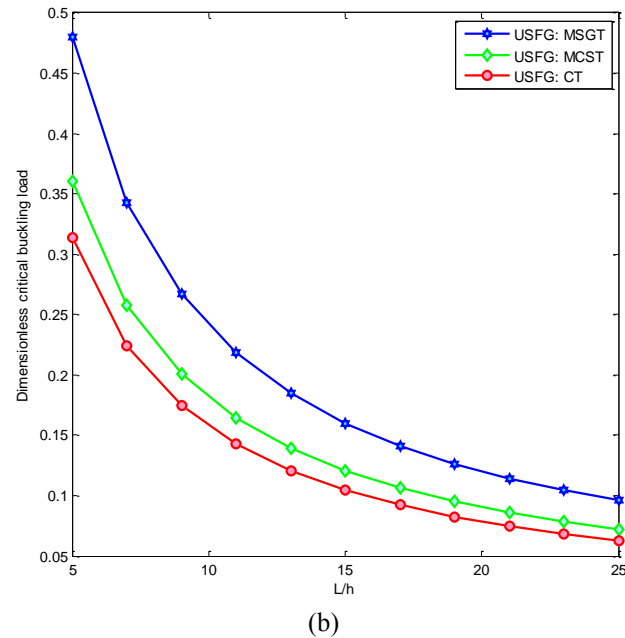


Fig. 5 Effects of material length scale parameters on (a) dimensionless nonlinear deflection (b) dimensionless critical buckling load

Fig. 5(a) and (b) show the effects of material length scale parameters on the dimensionless nonlinear deflection and the critical buckling load of the micro-composite beam reinforced by FG-SWBNNs based on MSGT, MCST and CT. It is observed from this figure that considering material length scale parameters lead to increase stiffness of the micro-composite Timoshenko beam, therefore the dimensionless deflection reduces absolute.

The effect of aspect ratio ( $L/h$ ) on the nonlinear deflection ratio for different amplitudes of the waviness UD micro composite beam for  $C-C$  boundary condition by MSGT is shown in Fig. 6. According to Fig. 6, the deflection ratio decreases with an increase in the aspect ratio. Also, with increasing amplitude of the waviness, the

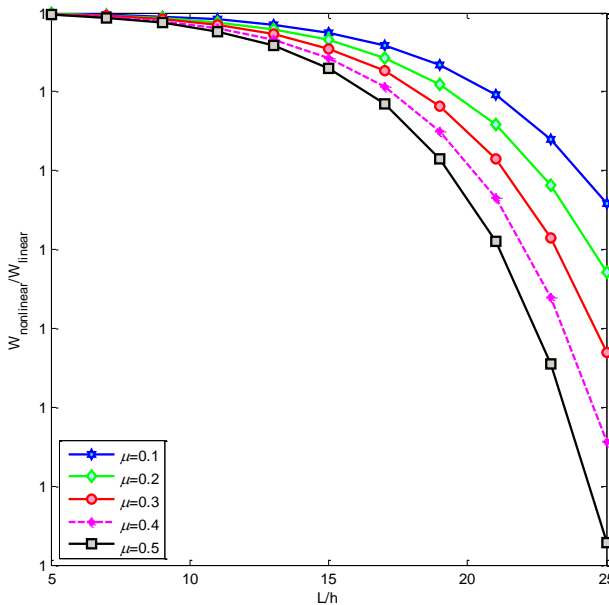


Fig. 6 The effect amplitudes of the waviness on the nonlinear maximum displacement for C-C boundary condition Timoshenko beam

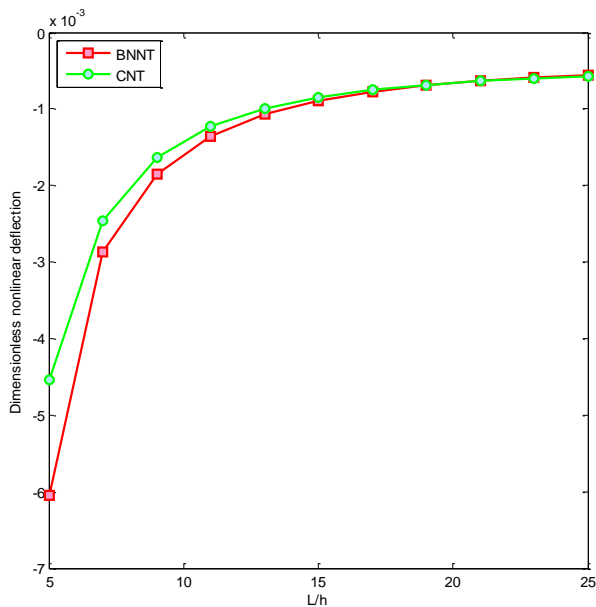


Fig. 7 Effects of various nanotubes on the dimensionless nonlinear deflection

nonlinear deflection ratio decreases. Since the effect of geometrical imperfection parameter on the system is nonlinear, with increasing of this parameter, the nonlinear stiffness of system increases and rigidity linear system does not change. Under these conditions, the nonlinear deflection of system reduces. In addition, as the amplitude of waviness  $\mu$  increases, the nonlinear are more sensitive to the von Kármán type nonlinearity  $(\frac{\partial w}{\partial x})^2$  in Eq. (5).

Figure 7 shows the effect of various nanotubes including BNNT and CNT for micro-composite beam on the dimensionless nonlinear deflection. It can be seen from this figure that the dimensionless nonlinear deflection for

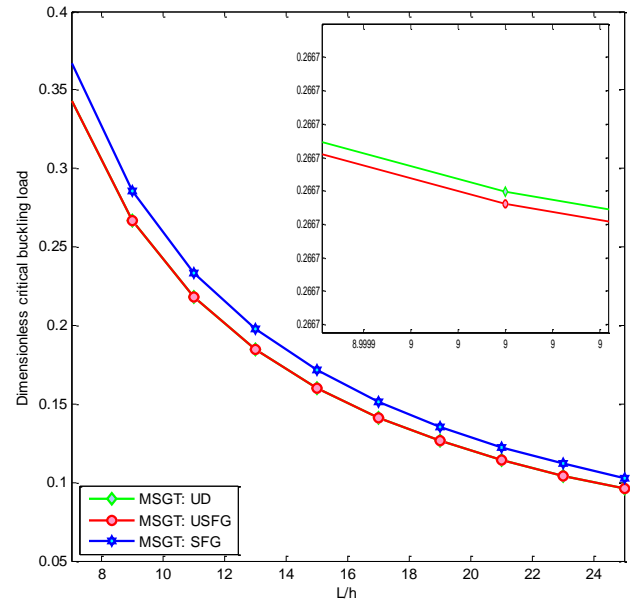


Fig. 8 Effects of FG-SWBNT distribution types on the dimensionless critical buckling load

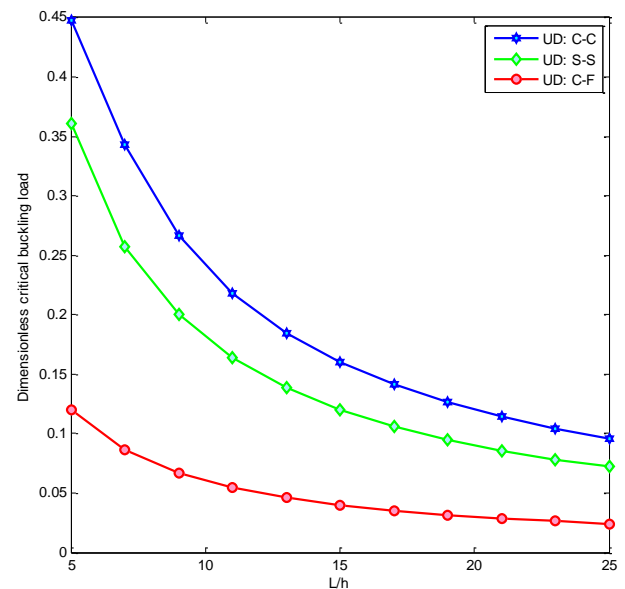


Fig. 9 Influence of various boundary conditions on the dimensionless critical buckling load

BNNT with considering the electric field is higher than that of for CNT with employing magnetic field. On the other hands, the micro-composite beam with considering BNNT becomes softer with respect to CNT.

Fig. 8 displays the effects of various distribution types of FG-SWBNT on the dimensionless critical buckling load of the micro-composite beam based on MSGT. According to this Figure, the critical buckling load decreases for all types of distribution with increasing the aspect ratio. It is obvious that the micro-composite beam is stiffer as reinforced by FG-X (SFG) distribution type rather than other distribution types (UD and FG-V (USFG)). Also it is observed that the value of dimensionless material length scale parameter plays more important role in the stiffness behavior of FG-SWBNT micro-composite beam.

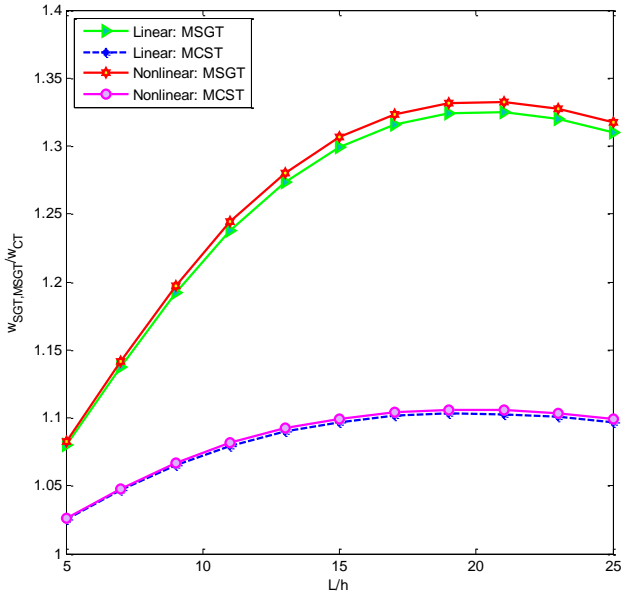


Fig. 10 The frequency ratio of micro composite beam for MSGT, MCST and CT

Fig. 9 depicts the effects of various boundary conditions on the dimensionless critical buckling load of the micro-composite beam reinforced by FG-SWBNNTs. In this figure, letter *C*, *S*, and *F* denote clamped, simply supported, and free boundary conditions in the edge of the micro-composite beam. As it is observed from Fig. 9 that the dimensionless critical buckling load for *C-C* and *C-F* have the lowest and highest values, respectively. Because of the clamped boundary condition with respect to simply supported and free boundary conditions leads to increase stiffer of the micro-composite beam.

6.2 Vibration of the micro-composite beam reinforced by FG-SWBNNTs

Based on various theories such as MSGT, MCST and CT, frequency ratio of the micro-composite beam are depicted for *C-C* boundary condition beam in Fig. 10. It can be seen that the model based on MSGT predicts the maximum value of nonlinear frequency ratio among various types of size-dependent effect. Also with increasing of aspect ratio for  $L/h > 8$ , the difference of frequency ratio between two cases increases and it cannot be ignored, while for  $L/h < 8$ , this results is not noticeable.

The effect of the elastic medium on the nonlinear frequency ratio is shown in Fig. 11. It is seen that for lower aspect ratio, a change of the elastic medium leads to increase the nonlinear frequency ratio of FG-SWBNNT micro-composite beam. It is noted that the elastic medium makes the FG-SWBNNT micro-composite beam model to be stiffer than without considering the elastic medium. Also in this figure, the slope of curves is not constant. These increases in the nonlinear frequency ratio versus the aspect ratio are found to be almost dependent on the change of the value of the elastic layer stiffness especially at higher values. At lower values of the elastic layer stiffness, this effect is not significant.

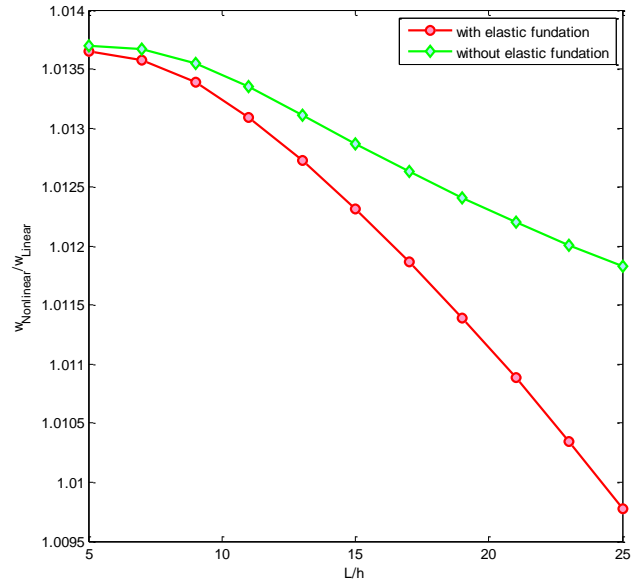


Fig. 11 The influence of elastic medium coefficient on the nonlinear frequency ratio

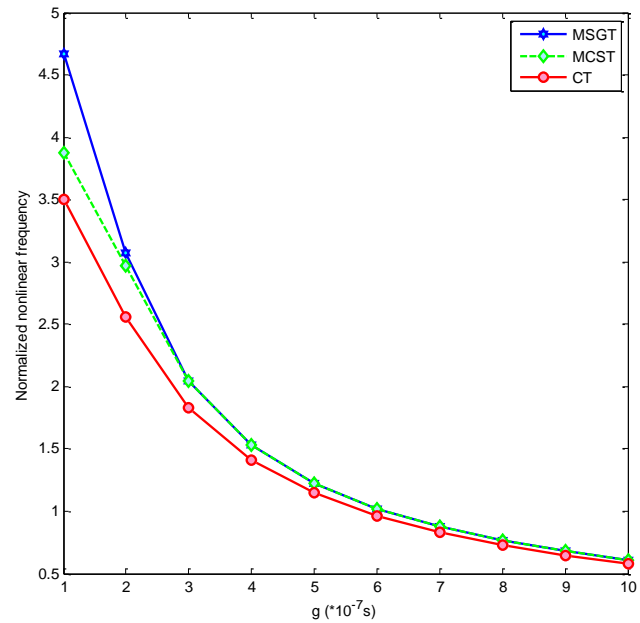


Fig. 12 The non-dimensional natural frequency versus the different structural damping coefficient for different theory

In Fig. 12, the variation of normalized nonlinear frequency with structural damping coefficient of visco-elastic micro-composite beam for classical and non-classical theories is depicted. It can be seen that the obtained dimensionless frequency by non-classical theories tends to have a greater reduction than with respect to the classical theory for structural damping coefficient. Also It can be observed in this figure that the difference between various theories is more obvious in  $g < 4$ .

Figs. 13 shows the first mode shape of buckling for various theories such as classical theory (CT), modified couple stress theory (MCST), and modified strain gradient theory (MSGT).

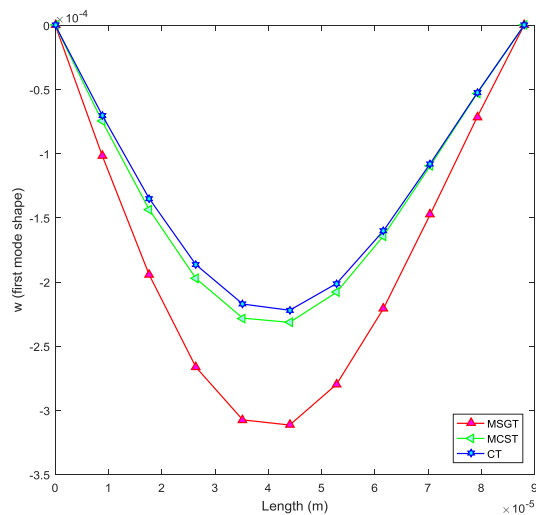


Fig. 13 The first mode shape of buckling for various theories

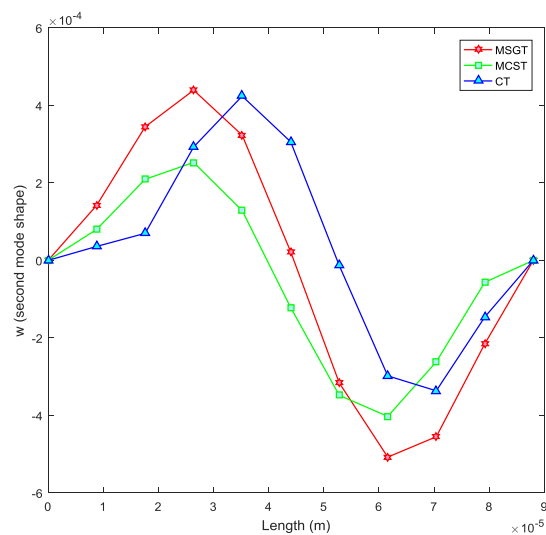


Fig. 14 The second mode shape of vibration for various theories

Also, Fig. 14 presents the second mode shape of vibration for various theories such as classical theory (CT), modified couple stress theory (MCST), and modified strain gradient theory (MSGT).

**7. Conclusions**

In this study, the nonlinear bending, buckling and vibration analysis of viscoelastic micro-composite beam reinforced by various distributions of BNNT with initial geometrical imperfection on elastic foundation is demonstrated. Then strain-displacement relations (kinematic equations) are calculated using the obtained displacement fields. MSGT is used to implement the size dependent effect at micro scale. Finally, the governing equations of motion for micro-composite beam are obtained using energy method and Hamilton’s principle. Nonlinear bending, critical buckling load and natural frequencies of micro-composite beam are calculated by employing FEM.

Also, the effects of variation values of UD, FG-V and FG-X distributions of BNNT, amplitudes of the waviness, various boundary conditions, material length scale parameter, damping coefficient, piezoelectric constant and elastic foundation on nonlinear maximum deflections, critical buckling load and natural frequency are illustrated. The results of this research can be listed as follows:

1. Number of elements required for convergence of the nonlinear bending and buckling micro-composite beam is equal to 30 and 40 elements, respectively.
2. With increasing dimensionless material length scale parameter, the nonlinear non-dimensional natural frequency and critical buckling load increases. Also, the nonlinear natural frequency and critical buckling load for MSGT is more than two other theories including MCST and CT. Increasing dimensionless material length scale parameter leads to increase in stiffness of system, so the natural frequency increases.
3. With increasing amplitude of the waviness, the nonlinear deflection decreases. So with increasing this parameter, the nonlinear stiffness of system increases and rigidity linear system does not change.
4. Increasing of the elastic foundation coefficients leads to increase in non-dimensional natural frequency.
5. With an increase in the BNNT volume fraction increases the nonlinear dimensionless natural frequency. Moreover, increasing BNNT volume fraction leads to increase in stiffness of micro composite beam model.
6. The clamped boundary condition with respect to simply supported and free boundary conditions leads to increase stiffer of the micro composite beam. Thus the dimensionless critical buckling load increases and vice versa for dimensionless deflection of micro-composite beam.
7. The nonlinear natural frequency and critical buckling load of micro-composite beam increases with an increase in the electrical field. Also, by increasing the imposed electrical field significantly increases the stability of the system that can behave as an actuator.
8. Micro-composite beam becomes stiffer with decreasing aspect ratio and the non-dimensional displacement of micro-composite beam reduces.
9. At specified value of aspect ratio, the dimensionless natural frequency and critical buckling load for FG-X micro-composite beam is more than the other state.
10. Imposed external voltage is an effective controlling parameter for dynamic stability of system.
11. The results revealed that the frequency was significantly influenced by the structural damping of the micro-composite beam, damping coefficient of elastic foundation.

**Acknowledgments**

The authors would like to thank the referees for their valuable comments. Also, they are thankful to the thank the Iranian Nanotechnology Development Committee for their financial support and the University of Kashan for supporting this work by Grant No. 463855/19.

## References

- Adnan Elshafei, M. (2013), "FE modeling and analysis of isotropic and orthotropic beams using first order shear deformation theory", *Mater. Sci. Appl.*, **4**(1), 77-102. <http://dx.doi.org/10.4236/msa.2013.41010>.
- Bakhadda, B., BachirBouiadjra, M., Bourada, F., Bousahla, A.A., Tounsi, A. and Mahmoud, S.R. (2018), "Dynamic and bending analysis of carbon nanotube-reinforced composite plates with elastic foundation", *Wind. Struct.*, **27**(5), 311-324. <https://doi.org/10.12989/was.2018.27.5.311>.
- Bellifa, H., Benrahou, K.H., Bousahla, A.A., Tounsi, A. and Mahmoud, S.R. (2017), "A nonlocal zeroth-order shear deformation theory for nonlinear postbuckling of nanobeams", *Struct. Eng. Mech.*, **62**(6), 695-702. <https://doi.org/10.12989/sem.2017.62.6.695>.
- Chakraborty, A., Mahapatra, D.R. and Gopalakrishnan, S. (2002), "Finite element analysis of free vibration and wave propagation in asymmetric composite beam with structural discontinuities", *Compos. Struct.*, **55**(1), 23-36. [https://doi.org/10.1016/S0263-8223\(01\)00130-1](https://doi.org/10.1016/S0263-8223(01)00130-1).
- Ghorbanpour Arani A., Hashemian M., Loghman A., and Mohammadimehr M. (2011b), "Study of dynamic stability of the double-walled carbon nanotubes under axial loading embedded in an elastic medium by the energy method", *J. Appl. Mech. Technical Physics*, **52**(5), 815-824. <https://doi.org/10.1134/S0021894411050178>.
- Ghorbanpour Arani A., Mohammadimehr M., Saidi A.R., Shogaei S. and Arefmanesh A. (2011a), "Thermal buckling analysis of double-walled carbon nanotubes considering the small-scale length effect", *Proc. IMechE, Part C, J. Mech. Eng. Sci.*, **225**(1), 248-256. <https://doi.org/10.1177/09544062JMES1975>.
- Ghorbanpour Arani, A. and Amir, S. (2013), "Electro-thermal vibration of visco-elastically coupled BNNT systems conveying fluid embedded on elastic foundation via strain gradient theory", *Physica B*, **419**, 1-6. <https://doi.org/10.1016/j.physb.2013.03.010>.
- Ghorbanpour Arani, A., Amir, S., Dashti, P. and Yousefi, M. (2014), "Flow-induced vibration of double bonded visco-CNTs under magnetic fields considering surface effect", *Comput. Mater. Sci.*, **86**, 144-154. <https://doi.org/10.1016/j.commatsci.2014.01.047>.
- Ghorbanpour Arani, A., Amir, S., Shajari, A.R. and Mozdianfard, M.R. (2012), "Electro-thermo-mechanical buckling of DWBNTs embedded in bundle of CNTs using nonlocal piezoelectricity cylindrical shell theory", *Compos. Part B: Engineering*, **43**(2), 195-203. <https://doi.org/10.1016/j.compositesb.2011.10.012>.
- Ghorbanpour Arani, A., Mobarakeh, M.R., Shams, S. and Mohammadimehr, M. (2012), "The effect of CNT volume fraction on the magneto-thermo-electro-mechanical behavior of smart nanocomposite cylinder", *J. Mech. Sci. Technol.*, **26**(8), 2565-2572. <https://doi.org/10.1007/s12206-012-0639-5>.
- Ghorbanpour Arani, A., Roustana Navia B. and Mohammadimehr, M. (2015), "Surface stress and agglomeration effects on nonlocal biaxial buckling polymeric nano-composite plate reinforced by CNT using various approaches", *Adv. Compos. Mater.*, **25**(5), 423-441. <https://doi.org/10.1080/09243046.2015.1052189>.
- Gu, X.J., Hao, Y.X., Zhang, W., Liu, L.T. and Chen, J. (2019), "Free vibration of rotating cantilever pre-twisted panel with initial exponential function type geometric imperfection", *Appl. Math. Model.*, **68**, 327-352. <https://doi.org/10.1016/j.apm.2018.11.037>.
- Heshmati, M. and Yas, M.H. (2013), "Dynamic analysis of functionally graded multi-walled carbon nanotube-polystyrene nanocomposite beams subjected to multi-moving loads", *Mater. Design*, **49**, 894-904. <https://doi.org/10.1016/j.matdes.2013.01.073>.
- Karami, B., Janghorban, M. and Tounsi, A. (2018a), "Nonlocal strain gradient 3D elasticity theory for anisotropic spherical nanoparticles", *Steel Compos Struct.*, **27**(2), 201-216. <https://doi.org/10.12989/scs.2018.27.2.201>.
- Karami, B., Janghorban, M. and Tounsi, A. (2018b), "Variational approach for wave dispersion in anisotropic doubly-curved nanoshells based on a new nonlocal strain gradient higher order shell theory", *Thin-Walled Struct.*, **129**, 251-264. <https://doi.org/10.1016/j.tws.2018.02.025>.
- Lam, D.C.C., Yang, F., Chong, A.C.M., Wang, J. and Tong, P. (2003), "Experiments and theory in strain gradient elasticity", *J. Mech. Phys. Solids*, **51**(8), 1477-1508. [https://doi.org/10.1016/S0022-5096\(03\)00053-X](https://doi.org/10.1016/S0022-5096(03)00053-X).
- Lei, Z.X., Zhang, L.W. and Liew, K.M. (2016), "Analysis of laminated CNT reinforced functionally graded plates using the element-free kp-Ritz method", *Compos. Struct.*, **84**, 211-221. <https://doi.org/10.1016/j.compositesb.2015.08.081>.
- Liew, K.M., Lei, Z.X. and Zhang, L.W. (2015), "Mechanical analysis of functionally graded carbon nanotube reinforced Composites: A review", *Compos. Struct.*, **120**, 90-97. <https://doi.org/10.1016/j.compstruct.2014.09.041>.
- Liew, K.M., Lei, Z.X., Yu, J.L. and Zhang, L.W. (2014), "Post buckling of carbon nanotube-reinforced functionally graded cylindrical panels under axial compression using a meshless approach", *Comput. Appl. Mech. Eng.*, **268**, 1-17. <https://doi.org/10.1016/j.cma.2013.09.001>.
- Mehar, K. and Panda, S.K. (2017), "Thermoelastic analysis of FG-CNT reinforced shear deformable composite plate under various loading", *Int. J. Comput. Meth.*, **14**(2). <https://doi.org/10.1142/S0219876217500190>.
- Mohammadimehr, M. and Rahmati, A.H. (2013), "Small scale effect on electro-thermo-mechanical vibration analysis of single-walled boron nitride nanorods under electric excitation", *Turkish J. Eng. Environ. Sci.*, **37**(1), 1-15.
- Mohammadimehr, M., Rostami, R. and Arefi, M. (2016f), "Electro-elastic analysis of a sandwich thick plate considering FG core and composite piezoelectric layers on Pasternak foundation using TSDT", *Steel Compos. Struct.*, **20**(3), 513-544.
- Mohammadimehr, M. and Shahedi, S. (2017b) "High-order buckling and free vibration analysis of two types sandwich beam including AL or PVC-foam flexible core and CNTs reinforced nanocomposite face sheets using GDQM", *Compos. Part B Eng.*, **108**, 91-107. <https://doi.org/10.1016/j.compositesb.2016.09.040>.
- Mohammadimehr, M. and Alimirzaei, S. (2016), "Nonlinear static and vibration analysis of Euler-Bernoulli composite beam model reinforced by FG-SWCNT with initial geometrical imperfection using FEM", *Struct. Eng. Mech.*, **59**(3), 431-454. <http://dx.doi.org/10.12989/sem.2016.59.3.431>.
- Mohammadimehr, M. and Alimirzaei, S. (2017), "Buckling and free vibration analysis of tapered FG- CNTRC micro Reddy beam under longitudinal magnetic field using FEM", *Smart Struct. Sys.*, **19**(3), 309-322. <https://doi.org/10.12989/sss.2017.19.3.309>.
- Mohammadimehr, M. and Mehrabi, M. (2017c), "Stability and free vibration analyses of double-bonded micro composite sandwich cylindrical shells conveying fluid flow", *Appl. Math. Model.*, **47**, 685-709. <https://doi.org/10.1016/j.apm.2017.03.054>.
- Mohammadimehr, M., Farahi, M.J. and Alimirzaei, S. (2016b), "Vibration and wave propagation analysis of twisted micro-beam using strain gradient theory", *Appl. Math. Mech.*, **37**(10), 1375-1392. <https://doi.org/10.1007/s10483-016-2138-9>.
- Mohammadimehr, M., Mohammadimehr, M.A. and Dashti, P. (2016c), "Size-dependent effect on biaxial and shear nonlinear buckling analysis of nonlocal isotropic and orthotropic micro-plate based on surface stress and modified couple stress theories using differential quadrature method (DQM)", *Appl. Math. Mech.*, **37**(4), 529-554. <https://doi.org/10.1007/s10483-016-2045-9>.

- Mohammadimehr, M., Mohandes, M. and Moradi, M., (2016a), "Size dependent effect on the buckling and vibration analysis of double-bonded nanocomposite piezoelectric plate reinforced by boron nitride nanotube based on modified couple stress theory", *J. Vib. Control.*, **22**(7), 1790-1807. <https://doi.org/10.1177/1077546314544513>.
- Mohammadimehr, M., Rousta Navi, B. and Ghorbanpour Arani, A. (2015), "Free vibration of viscoelastic double-bonded polymeric nanocomposite plates reinforced by FG-SWCNTs using MSGT, sinusoidal shear deformation theory and meshless method", *Compos. Struct.*, **131**, 654-671. <https://doi.org/10.1016/j.compstruct.2015.05.077>.
- Mohammadimehr, M., Rousta Navi, B. and Ghorbanpour Arani, A. (2016d), "Modified strain gradient Reddy rectangular plate model for biaxial buckling and bending analysis of double-coupled piezoelectric polymeric nanocomposite reinforced by FG-SWCNT", *Compos. Part. B.*, **87**, 132-148. <https://doi.org/10.1016/j.compositesb.2015.10.007>.
- Mohammadimehr, M., Saidi, A.R., Ghorbanpour Arani, A., Arefmanesh, A. and Han, Q. (2010), "Torsional buckling of a DWCNT embedded on Winkler and Pasternak Foundations using nonlocal theory", *J. Mech. Sci.*, **24**(6), 1289-1299. <https://doi.org/10.1007/s12206-010-0331-6>.
- Mohammadimehr, M., Salemi, M. and Rousta Navi, B. (2016e), "Bending, buckling, and free vibration analysis of MSGT microcomposite Reddy plate reinforced by FG-SWCNTs with temperature-dependent material properties under hydro-thermo-mechanical loadings using DQM", *Compos. Struct.*, **138**, 361-380. <https://doi.org/10.1016/j.compstruct.2015.11.055>.
- Mohammadimehr, M., Zarei, H. B., Parakandeh, A. and Arani, A.G. (2017b), "Vibration analysis of double-bonded sandwich microplates with nanocomposite facesheets reinforced by symmetric and un-symmetric distributions of nanotubes under multi physical fields", *Struct. Eng. Mech.*, **64**(3), 361-379. <https://doi.org/10.12989/sem.2017.64.3.361>.
- Moradi, R., Foroutan M. and Poursasghar, A. (2013), "Dynamic analysis of functionally graded nanocomposite cylinders reinforced by carbon nanotube by a mesh-free method", *Mater. Design*, **44**, 256-266. <https://doi.org/10.1016/j.matdes.2012.07.069>.
- Mosallaie Barzok, A.A., Ghorbanpour Arani, A., Kolahchi, R. and Mozdianfard, M.R. (2012), "Electro-thermo-mechanical torsional buckling of a piezoelectric polymeric cylindrical shell reinforced by DWBNNTs with an elastic core", *Appl. Math. Model.*, **36**, 2983-2995. <https://doi.org/10.1016/j.apm.2011.09.093>.
- Murmu, T. and Pradhan, S.C. (2009), "Buckling analysis of a single-walled carbon nanotube embedded in an elastic medium based on nonlocal elasticity and Timoshenko beam theory and using DQM", *Physica. E.*, **41**(7), 1232-1239. <https://doi.org/10.1016/j.physe.2009.02.004>.
- Narendar, S., Gupta, S.S. and Gopalakrishnan, S. (2012), "Wave propagation in single-walled carbon nanotube under longitudinal magnetic field using nonlocal Euler-Bernoulli beam theory", *Appl. Math. Model.*, **36**(9), 4529-4538. <https://doi.org/10.1016/j.apm.2011.11.073>.
- Nirmala, V. and Kolandaivel, P. (2007), "Structure and electronic properties of armchair boron nitride nanotubes", *J. Molecular Struct.*, **817**(1-3), 137-145. <https://doi.org/10.1016/j.theochem.2007.04.033>.
- Oh, E. (2011), "Elastic properties of various boron-nitride structures", *Met. Mater. Int.*, **17**(1), 21-27. <https://doi.org/10.1007/s12540-011-0204-2>.
- Reddy, J.N. (2004), *An Introduction to nonlinear finite element analysis*, New York, Oxford University Press, USA.
- Salehi-Khojin, M. and Jalili, N. (2008), "Buckling of boron nitride nanotube reinforced piezoelectric polymeric composites subject to combined electro-thermo-mechanical loadings", *Compos. Sci. Tech.*, **68**(6), 1489-1501. <https://doi.org/10.1016/j.compscitech.2007.10.024>.
- Vaccarini, L., Goze, C., Henrard, L., Hernandez, E., Bernier, P. and Rubio, A. (2000), "Mechanical and Electronic Properties of Carbon and Boron-Nitride Nanotubes", *Carbon*, **38**, 1681. [https://doi.org/10.1016/S0008-6223\(99\)00293-6](https://doi.org/10.1016/S0008-6223(99)00293-6).
- Wang, B., Deng, Z.C. and Zhang, K. (2013), "Nonlinear vibration of embedded single-walled carbon nanotube with geometrical imperfection under harmonic load based on nonlocal Timoshenko beam theory", *Appl. Math. Mech.*, **34**(3), 269-280. <https://doi.org/10.1007/s10483-013-1669-8>.
- Wang, B., Zichen, D., Huajiang, O. and Jiayi, Z. (2015), "Wave propagation analysis in nonlinear curved single-walled carbon nanotubes based on nonlocal elasticity theory", *Physica. E.*, **66**, 283-292. <https://doi.org/10.1016/j.physe.2014.09.015>.
- Yas, M.H. and Samadi, N. (2012), "Free vibrations and buckling analysis of carbon nanotube-reinforced composite Timoshenko beams on elastic foundation", *Int. J. Pres. Ves. Pip.*, **98**, 119-128. <https://doi.org/10.1016/j.ijpvp.2012.07.012>.
- Yas, M.H. and Heshmati, M. (2012), "Dynamic analysis of functionally graded nano composite beams reinforced by randomly oriented carbon nanotube under the action of moving load", *Appl. Math. Model.*, **36**(4), 1371-1394. <https://doi.org/10.1016/j.apm.2011.08.037>.
- Zhang, B., He, Y., Liu, D., Gan, Z. and Shen, L. (2014), "Non-classical Timoshenko beam element based on the strain gradient elasticity theory", *Finite Elem. Anal. Des.*, **79**, 22-39. <https://doi.org/10.1016/j.finel.2013.10.004>.
- Zhang, L.W. and Selim, B.A. (2017), "Vibration analysis of CNT-reinforced thick laminated composite plates based on Reddy's higher-order shear deformation theory", *Compos. Struct.*, **160**, 689-705. <https://doi.org/10.1016/j.compstruct.2016.10.102>.
- Zhang, L.W. and Xiao, L.N. (2016), "Mechanical behavior of laminated CNT-reinforced composite skew plates subjected to dynamic loading", *Compos. Struct.*, **122**, 219-230. <https://doi.org/10.1016/j.compositesb.2017.03.041>.
- Zhang, L.W., Liew, K.M. and Reddy, J.N. (2016), "Postbuckling of carbon nanotube reinforced functionally graded plates with edges elastically restrained against translation and rotation under axial compression", *Compos. Struct.*, **298**, 1-28. <https://doi.org/10.1016/j.cma.2015.09.016>.
- Zhang, L.W., Song, G. and Liew, K.M. (2015), "Nonlinear bending analysis of FG-CNT reinforced composite thick plates resting on Pasternak foundations using the element-free IMLS-Ritz method", *Compos. Struct.*, **128**, 165-175. <https://doi.org/10.1016/j.compstruct.2015.03.011>.
- Zhang, L.W., Song, Z.G. and Liew, K.M. (2016), "Optimal shape control of CNT reinforced functionally graded composite plates using piezoelectric patches", *Compos. part B*, **85**, 140-149. <https://doi.org/10.1016/j.compositesb.2015.09.044>.
- Zhang, L.W., Liu, W.H. and Liew, K.M. (2016), "Geometrically nonlinear large deformation analysis of triangular CNT-reinforced composite plates", *Int. J. Non-Linear Mech.*, **6**, 122-132. <https://doi.org/10.1016/j.ijnonlinmec.2016.08.004>.
- Zhang, L.W., Zhu, P. and Liew, K.M. (2013), "Thermal buckling of functionally graded plates using a local Kriging meshless method", *Compos. Struct.*, **108**, 472-492. <https://doi.org/10.1016/j.compstruct.2013.09.043>.
- Zhu, P., Zhang, L.W. and Liew, K.M. (2014), "Geometrically nonlinear thermomechanical analysis of moderately thick functionally graded plates using a local PetrovGalerkin approach with moving Kriging interpolation", *Compos. Struct.*, **107**(4), 298-314. <https://doi.org/10.1016/j.compstruct.2013.08.001>.

## Appendix A

$$\begin{aligned}
N_1 &= 1 - \frac{x}{l_e}, & N_2 &= -(6\hat{c}_1)x + \left(\frac{6\hat{c}_1}{l_e}\right)x^2, & N_3 &= (3\hat{c}_1 l_e)x - (3\hat{c}_1)x^2 \\
N_4 &= \frac{x}{l_e}, & N_5 &= (6\hat{c}_1)x - \left(\frac{6\hat{c}_1}{l_e}\right)x^2, & N_6 &= (3\hat{c}_1 l_e)x - (3\hat{c}_1)x^2 \\
N_7 &= 1 - \left(\frac{\hat{c}_2}{l_e}\right)x - (3\hat{c}_3)x^2 + \left(\frac{2\hat{c}_3}{l_e}\right)x^3, & N_8 &= (\hat{c}_5)x + \left(\frac{2\hat{c}_4}{l_e}\right)x^2 - (\hat{c}_3)x^3 \\
N_9 &= \left(\frac{\hat{c}_2}{l_e}\right)x + (3\hat{c}_3)x^2 - \left(\frac{2\hat{c}_3}{l_e}\right)x^3, & N_{10} &= -\left(\frac{1}{2}\hat{c}_2\right)x + \left(\frac{\hat{c}_6}{l_e}\right)x^2 - (\hat{c}_3)x^3 \\
N_{11} &= (6\hat{c}_3)x - \left(\frac{6\hat{c}_3}{l_e}\right)x^2, & N_{12} &= 1 + \left(\frac{\hat{c}_7}{l_e}\right)x + (3\hat{c}_3)x^2 \\
N_{13} &= -(6\hat{c}_3)x + \left(\frac{6\hat{c}_3}{l_e}\right)x^2, & N_{14} &= -\left(\frac{\hat{c}_8}{l_e}\right)x + (3\hat{c}_3)x^2 \\
N_{15} &= \left(1 - \frac{x}{l_e}\right)\left(\frac{1}{2} + \frac{z}{h}\right), & N_{16} &= \left(\frac{x}{l_e}\right)\left(\frac{1}{2} - \frac{z}{h}\right)
\end{aligned} \tag{A.1}$$

where

$$\begin{aligned}
\hat{c}_1 &= \frac{A_{11}^1 B_{11}^0 k_s}{(k_s l_e^2 B_{11}^0 A_{11}^0 + 12A_{11}^2 A_{11}^0 - 12(A_{11}^1)^2)}, & c_2 &= \frac{(12A_{11}^0 A_{11}^2 - 12(A_{11}^1)^2)}{(k_s l_e^2 B_{11}^0 A_{11}^0 + 12A_{11}^2 A_{11}^0 - 12(A_{11}^1)^2)} \\
\hat{c}_3 &= \frac{k_s B_{11}^0 A_{11}^0}{(k_s l_e^2 B_{11}^0 A_{11}^0 + 12A_{11}^2 A_{11}^0 - 12(A_{11}^1)^2)}, & c_4 &= \frac{(k_s l_e^2 B_{11}^0 A_{11}^0 + 6A_{11}^2 A_{11}^0 - 6(A_{11}^1)^2)}{(k_s l_e^2 B_{11}^0 A_{11}^0 + 12A_{11}^2 A_{11}^0 - 12(A_{11}^1)^2)} \\
\hat{c}_5 &= -\frac{(k_s l_e^2 B_{11}^0 A_{11}^0 + 3A_{11}^2 A_{11}^0 - 3(A_{11}^1)^2)}{(k_s l_e^2 B_{11}^0 A_{11}^0 + 12A_{11}^2 A_{11}^0 - 12(A_{11}^1)^2)}, & c_6 &= \frac{(k_s l_e^2 B_{11}^0 A_{11}^0 - 6A_{11}^2 A_{11}^0 + 6(A_{11}^1)^2)}{(k_s l_e^2 B_{11}^0 A_{11}^0 + 12A_{11}^2 A_{11}^0 - 12(A_{11}^1)^2)} \\
\hat{c}_7 &= \frac{(-4k_s l_e^2 B_{11}^0 A_{11}^0 - 12A_{11}^2 A_{11}^0 + 12(A_{11}^1)^2)}{(k_s l_e^2 B_{11}^0 A_{11}^0 + 12A_{11}^2 A_{11}^0 - 12(A_{11}^1)^2)}, & \hat{c}_8 &= \frac{(2k_s l_e^2 B_{11}^0 A_{11}^0 - 12A_{11}^2 A_{11}^0 + 12(A_{11}^1)^2)}{(k_s l_e^2 B_{11}^0 A_{11}^0 + 12A_{11}^2 A_{11}^0 - 12(A_{11}^1)^2)}
\end{aligned} \tag{A.2}$$

## Appendix B

### ➤ Element stiffness matrices

$$\begin{aligned}
 K_{11}^{ij} &= \int_{x_a}^{x_b} A_{11}^0 \frac{dN_{ui}}{dx} \frac{dN_{uj}}{dx} dx + \int_{x_a}^{x_b} (2l_0^2 + \frac{4}{5}l_1^2) D_{11}^0 \frac{d^2N_{ui}}{dx^2} \frac{d^2N_{uj}}{dx^2} dx \\
 K_{12}^{ij} &= \int_{x_a}^{x_b} (\mu + \frac{1}{2}) A_{11}^0 \frac{dN_{ui}}{dx} \frac{dN_{wj}}{dx} (\frac{dw}{dx}) dx + \int_{x_a}^{x_b} (2l_0^2 + \frac{4}{5}l_1^2) (2\mu + 1) D_{11}^0 \frac{d^2N_{ui}}{dx^2} \frac{d^2N_{wj}}{dx^2} (\frac{dw}{dx}) dx \\
 K_{13}^{ij} &= \int_{x_a}^{x_b} A_{11}^1 \frac{dN_{ui}}{dx} \frac{dN_{\psi j}}{dx} dx + \int_{x_a}^{x_b} (2l_0^2 + \frac{4}{5}l_1^2) D_{11}^1 \frac{d^2N_{ui}}{dx^2} \frac{d^2N_{\psi j}}{dx^2} dx \\
 K_{14}^{ij} &= \int_x m_0 \frac{dN_{ui}}{dx} \frac{dN_{\phi j}}{dx} dx
 \end{aligned} \tag{B.1}$$

$$\begin{aligned}
 K_{21}^{ij} &= 2 \int_x (\mu + \frac{1}{2}) A_{11}^0 \frac{dN_{wi}}{dx} \frac{dN_{uj}}{dx} (\frac{\partial w}{\partial x}) dx + \int_x (2l_0^2 + \frac{4}{5}l_1^2) (2\mu + 1) D_{11}^0 \frac{d^2N_{wi}}{dx^2} \frac{d^2N_{uj}}{dx^2} (\frac{\partial w}{\partial x}) dx \\
 &+ \int_x (2l_0^2 + \frac{4}{5}l_1^2) (2\mu + 1) D_{11}^0 \frac{dN_{wi}}{dx} \frac{d^2N_{uj}}{dx^2} (\frac{\partial^2 w}{\partial x^2}) dx \\
 K_{22}^{ij} &= \int_{x_a}^{x_b} k_s B_{11}^0 \frac{dN_{wi}}{dx} \frac{dN_{wj}}{dx} dx + \int_{x_a}^{x_b} (\frac{8}{15}l_1^2 + \frac{1}{4}l_2^2) D_{11}^0 \frac{d^2N_{wi}}{dx^2} \frac{d^2N_{wj}}{dx^2} dx \\
 &+ b \int_{x_a}^{x_b} k_w N_{wi} N_{wj} dx - b \int_{x_a}^{x_b} k_g N_{wi} \frac{d^2N_{wj}}{dx^2} dx - b \int_{x_a}^{x_b} \mu_1 H_x^2 N_{wi} \frac{d^2N_{wj}}{dx^2} dx \\
 &+ 2 \int_{x_a}^{x_b} (\mu + \frac{1}{2})^2 A_{11}^0 \frac{dN_{wi}}{dx} \frac{dN_{wj}}{dx} (\frac{dw}{dx})^2 dx + \int_{x_a}^{x_b} (2\mu + 1)^2 (2l_0^2 + \frac{4}{5}l_1^2) D_{11}^0 \frac{d^2N_{wi}}{dx^2} \frac{d^2N_{wj}}{dx^2} (\frac{dw}{dx})^2 dx \\
 &+ \int_{x_a}^{x_b} (2\mu + 1)^2 (2l_0^2 + \frac{4}{5}l_1^2) D_{11}^0 \frac{dN_{wi}}{dx} \frac{d^2N_{wj}}{dx^2} (\frac{dw}{dx}) (\frac{dw}{dx})^2 dx
 \end{aligned} \tag{B.2}$$

$$\begin{aligned}
 K_{23}^{ij} &= \int_{x_a}^{x_b} k_s B_{11}^0 \frac{\partial N_{wi}}{\partial x} N_{\psi j} dx + \int_{x_a}^{x_b} (\frac{16}{15}l_1^2 - \frac{1}{4}l_2^2) D_{11}^0 \frac{d^2N_{wi}}{dx^2} \frac{dN_{\psi j}}{dx} dx + \\
 &+ 2 \int_{x_a}^{x_b} (\mu + \frac{1}{2}) A_{11}^1 \frac{dN_{wi}}{dx} \frac{dN_{\psi j}}{dx} (\frac{dw}{dx}) dx + \int_{x_a}^{x_b} (2\mu + 1) (2l_0^2 + \frac{4}{5}l_1^2) D_{11}^1 \frac{d^2N_{wi}}{dx^2} \frac{d^2N_{\psi j}}{dx^2} (\frac{dw}{dx}) dx \\
 &+ \int_{x_a}^{x_b} (2\mu + 1) (2l_0^2 + \frac{4}{5}l_1^2) D_{11}^1 \frac{dN_{wi}}{dx} \frac{d^2N_{\psi j}}{dx^2} (\frac{\partial^2 w}{\partial x^2}) dx \\
 K_{24}^{ij} &= 2 \int_{x_a}^{x_b} (\mu + \frac{1}{2}) m_0 \frac{dN_{wi}}{dx} \frac{dN_{\phi j}}{dx} (\frac{dw}{dx}) dx
 \end{aligned}$$

$$\begin{aligned}
 K_{31}^{ij} &= \int_{x_a}^{x_b} A_{11}^1 \frac{dN_{\psi i}}{dx} \frac{dN_{uj}}{dx} dx + \int_{x_a}^{x_b} (2l_0^2 + \frac{4}{5}l_1^2) D_{11}^1 \frac{d^2N_{\psi i}}{dx^2} \frac{d^2N_{uj}}{dx^2} dx \\
 K_{32}^{ij} &= \int_{x_a}^{x_b} k_s B_{11}^0 N_{\psi i} \frac{\partial N_{wj}}{\partial x} dx + \int_{x_a}^{x_b} (\frac{16}{15}l_1^2 - \frac{1}{4}l_2^2) D_{11}^0 \frac{dN_{\psi i}}{dx} \frac{d^2N_{wj}}{dx^2} dx \\
 &+ \int_{x_a}^{x_b} (\mu + \frac{1}{2}) A_{11}^1 \frac{dN_{\psi i}}{dx} \frac{dN_{wj}}{dx} (\frac{dw}{dx}) dx + \int_{x_a}^{x_b} (2\mu + 1) (2l_0^2 + \frac{4}{5}l_1^2) D_{11}^1 \frac{d^2N_{\psi i}}{dx^2} \frac{d^2N_{wj}}{dx^2} (\frac{dw}{dx}) dx \\
 K_{33}^{ij} &= \int_x k_s B_{11}^0 N_{\psi i} N_{\psi j} dx + \int_x A_{11}^2 \frac{dN_{\psi i}}{dx} \frac{dN_{\psi j}}{dx} dx + \\
 &+ \int_x (2l_0^2 + \frac{32}{15}l_1^2 + \frac{1}{4}l_2^2) D_{11}^0 \frac{dN_{\psi i}}{dx} \frac{dN_{\psi j}}{dx} dx + \int_x (2l_0^2 + \frac{4}{5}l_1^2) D_{11}^2 \frac{d^2N_{\psi i}}{dx^2} \frac{d^2N_{\psi j}}{dx^2} dx \\
 K_{34}^{ij} &= \int_x m_1 \frac{dN_{\psi i}}{dx} \frac{dN_{\phi j}}{dx} dx
 \end{aligned} \tag{B.3}$$

$$\begin{aligned}
K_{41}^{ij} &= \int_x m_0 \frac{dN_{\varphi i}}{dx} \frac{dN_{\psi j}}{dx} dx \\
K_{42}^{ij} &= \int_{x_a}^{x_b} \left(\mu + \frac{1}{2}\right) m_0 \frac{dN_{\varphi i}}{dx} \frac{dN_{w j}}{dx} \left(\frac{dw}{dx}\right) dx \\
K_{43}^{ij} &= \int_x m_1 \frac{dN_{\varphi i}}{dx} \frac{dN_{\psi j}}{dx} dx \\
K_{44}^{ij} &= - \int_x m_2 \frac{\partial N_{\varphi i}}{\partial x} \frac{\partial N_{\psi j}}{\partial x} dx
\end{aligned} \tag{B.4}$$

➤ Element mass matrices

$$\begin{aligned}
M_{11}^{ij} &= \int_{x_a}^{x_b} I_0 N_{u i} N_{u j} dx, \quad M_{12} = 0, \quad M_{13} = \int_{x_a}^{x_b} I_1 N_{u i} N_{\psi j} dx \\
M_{21} &= 0, \quad M_{22} = \int_{x_a}^{x_b} I_0 N_{w i} N_{w j} dx, \quad M_{23} = 0 \\
M_{31} &= \int_{x_a}^{x_b} I_1 N_{\psi i} N_{u j} dx, \quad M_{32} = 0, \quad M_{33} = \int_{x_a}^{x_b} I_2 N_{\psi i} N_{\psi j} dx
\end{aligned} \tag{B.5}$$

➤ The coefficient of stability matrix can be written as

$$[G] = P_M \int_{x_a}^{x_b} \frac{dN_{w i}}{dx} \frac{dN_{w j}}{dx} dx \tag{B.6}$$

➤ Element damping matrix

$$\begin{aligned}
C_{11}^{ij} &= \int_{x_a}^{x_b} g A_{11}^0 \frac{dN_{u i}}{dx} \frac{dN_{u j}}{dx} dx, \quad C_{12}^{ij} = 2 \int_{x_a}^{x_b} g A_{11}^0 \left(\mu + \frac{1}{2}\right) \frac{dN_{u i}}{dx} \frac{dN_{w j}}{dx} \left(\frac{dw}{dx}\right) dx \\
C_{13}^{ij} &= \int_{x_a}^{x_b} g A_{11}^1 \frac{dN_{u i}}{dx} \frac{dN_{\psi j}}{dx} dx, \quad C_{21}^{ij} = 2 \int_{x_a}^{x_b} g A_{11}^0 \left(\mu + \frac{1}{2}\right) \frac{dN_{w i}}{dx} \frac{dN_{u j}}{dx} \left(\frac{dw}{dx}\right) dx \\
C_{22}^{ij} &= \int_{x_a}^{x_b} k_s g B_{11}^0 \frac{dN_{w i}}{dx} \frac{dN_{w j}}{dx} dx + 4 \int_{x_a}^{x_b} \left(\mu + \frac{1}{2}\right)^2 g A_{11}^0 \frac{dN_{w i}}{dx} \frac{dN_{w j}}{dx} \left(\frac{dw}{dx}\right)^2 dx \\
C_{23}^{ij} &= \int_{x_a}^{x_b} k_s g B_{11}^0 \frac{dN_{w i}}{dx} N_{\psi j} dx + 2 \int_{x_a}^{x_b} g A_{11}^1 \left(\mu + \frac{1}{2}\right) \frac{dN_{w i}}{dx} \frac{dN_{\psi j}}{dx} \left(\frac{dw}{dx}\right) dx \\
C_{31}^{ij} &= \int_{x_a}^{x_b} g A_{11}^1 \frac{dN_{\psi i}}{dx} \frac{dN_{u j}}{dx} dx \\
C_{32}^{ij} &= \int_{x_a}^{x_b} k_s g B_{11}^0 N_{\psi i} \frac{dN_{w j}}{dx} dx + 2 \int_{x_a}^{x_b} g A_{11}^1 \left(\mu + \frac{1}{2}\right) \frac{dN_{\psi i}}{dx} \frac{dN_{w j}}{dx} \left(\frac{dw}{dx}\right) dx \\
C_{33}^{ij} &= \int_{x_a}^{x_b} A_{11}^2 g \frac{dN_{\psi i}}{dx} \frac{dN_{\psi j}}{dx} dx + \int_{x_a}^{x_b} k_s g B_{11}^0 N_{\psi i} N_{\psi j} dx
\end{aligned} \tag{B.7}$$